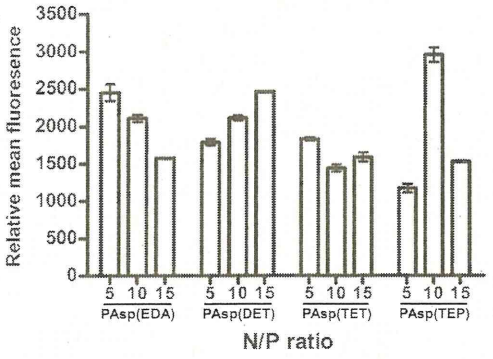

Figure 7. Cellular uptake of Cy5-labeled pDNA complexed with N-substituted polyaspartamides at various N/P ratios after 24 h incubation with Huh-7 cells (10 000 cells). Results are expressed as mean ± SEM ($N = 4$).

N/P = 5 and other N-substituted polyaspartamides except PAsp(TEP) at N/P = 15 were observed ($P < 0.01$). Polyplexes from PAsp(TEP) showed significantly lower cell viability than those from PAsp(DET) and PAsp(TET) at N/P = 15 ($P < 0.01$), indicating higher cytotoxicity with an increase in the N/P ratio.

Cellular Uptake of Polyplexes Determined by Flow Cytometry. The transfection efficiency of the polyplexes is often correlated with their cellular uptake. Thus, we compared the cellular uptake of each polyplex containing Cy5-labeled pDNA using flow cytometry. The histogram of flow cytometry revealed that almost 100% of the cells underwent polyplex uptake (data not shown). Figure 7 shows the relative mean fluorescence for the cellular uptake of Cy5-labeled pDNA, which apparently does not correlate with the transfection efficiency (Figure 5). Indeed, despite the significantly lower transfection efficiency, the polyplexes from PAsp(EDA) and PAsp(TET) showed levels of cellular uptake similar to those from PAsp(DET) and PAsp(TEP).

Intracellular Trafficking of Polyplexes Observed by Confocal Laser Scanning Microscopy (CLSM). Intracellular trafficking of each polyplex (N/P = 10) containing Cy5-labeled pDNA (red) was monitored particularly for endosomal localization by CLSM after staining the late endosome and lysosome with LysoTracker Green (green) and the nucleus with Hoechst 33342 (blue) (Figure 8a,b). In the overlay images, the yellow pixels represent the colocalization of Cy5-labeled pDNA with the late endosome/lysosome. Note that in our previous CLSM study Cy5-labeled pDNA in the poly(L-lysine) polyplex, which was used as the negative control and lacks endosomal escape ability, was found to maintain colocalization with the late endosome/lysosome throughout the observation period. This result provided the basis for estimating the endosomal escape ability of examined polyplexes from the decrease in the colocalization ratio estimated from the CLSM data.[26] Eventually, PAsp(DET) and PAsp(TEP) polyplexes appeared to disperse more efficiently in the entire cytoplasmic region than other polyplexes from the polymers with the odd-numbered repeating aminoethylene units in the side chains. As shown in Figure 8c, PAsp(EDA) and PAsp(TET) polyplexes showed an increase in the colocalization ratio until 12 and 24 h, respectively, indicating that the major fraction of PA-O polyplexes might be trapped in the lysosome. In contrast, PAsp(DET) and PAsp(TEP) polyplexes showed colocalization ratios lower than those of PAsp(EDA) and PAsp(TET) polyplexes at all time points. Also, PAsp(DET) and PAsp(TEP) polyplexes showed a decrease in the colocalization ratio after 12 and 6 h incubation, respectively, suggesting that the major fraction of PA-E polyplexes might escape from the endosome. At 12 h, the colocalization ratio of PAsp(DET) polyplexes was significantly lower than those of PAsp(EDA) and PAsp(TET) polyplexes ($P < 0.05$). At 24 and 48 h, the colocalization ratio of PAsp(TEP) polyplexes was significantly lower than that of PAsp(DET) polyplexes ($P < 0.05$ at 24 h, $P < 0.01$ at 48 h), indicating that the most efficient endosomal escape was for PAsp(TEP) polyplexes. Furthermore, the Manders coefficients were calculated using Image J software (http://rsbweb.nih.gov/ij/) to evaluate the colocalization of Cy5-labeled pDNA and LysoTracker after 48 h incubation. Note that the coefficients range between 0 and 1, which indicates no overlap and full overlap, respectively, and a higher value indicates that a larger fraction of polyplexes is trapped in the endosome/lysosome. The coefficients were calculated to be 0.549 for PAsp(EDA), 0.381 for PAsp(DET), 0.498 for PAsp(TET), and 0.345 for PAsp(TEP), consistent with the endosome colocalization ratios in Figure 8c. From these results, we conclude that the polyplexes from the polymer possessing the even-numbered repeating aminoethylene units enable the efficient endosomal escape of complexed pDNA into the cytoplasm, which agrees well with the transfection results shown in Figure 5.

DISCUSSION

In this study, to elucidate the precise structure–function relationship of the polyplexes, we synthesized a series of N-substituted polyaspartamides with increasing numbers of repeating aminoethylene units in the side chain: PAsp(EDA), PAsp(DET), PAsp(TET), and PAsp(TEP) (one to four repeating aminoethylene unit(s), respectively). The polyplexes from these N-substituted polyaspartamides were confirmed to have a similar size (~100 nm) and ζ-potential (~30 mV) at N/P ratios >4 (Figure 2, Supporting Information), suggesting similar fundamental physicochemical properties. The in vitro transfection experiment with Huh-7 cells exhibited a distinctive odd–even effect with respect to the number of repeating aminoethylene units: the polyplexes from the polymer with the even-numbered repeating aminoethylene units (PA-E) showed appreciably higher transfection efficiencies without marked cytotoxicity compared to polymers with odd-numbered repeating aminoethylene units (PA-O) (Figures 5 and 6).

To elucidate the reasons for this unique odd–even effect, we examined the cytotoxicity, cellular uptake, and endosomal escape behaviors of each polyplex. While the cell viability (Figure 6) and cellular uptake (Figure 7) profiles were similar between the polyplexes from both PA-E and PA-O, a significant difference in the endosomal escape behavior as determined from CLSM imagery was observed between the two variants. PA-E [PAsp(DET) and PAsp(TEP)] polyplexes revealed lower endosomal colocalization and higher dispersion into the cytoplasm than PA-O [PAsp(EDA) and PAsp(TET)] polyplexes (Figure 8), indicating that the higher transfection efficiency of the PA-E polyplexes is strongly correlated with their capability of endosomal escape.

Several previous studies revealed that the endosomal escape of the polyplexes may be facilitated by an increased osmotic pressure in the endosome because of a buffering effect associated with the amino groups in the constituent polycations (proton sponge hypothesis).[12,17] Accordingly, we examined the relationship between the buffering capacity of amino groups in the

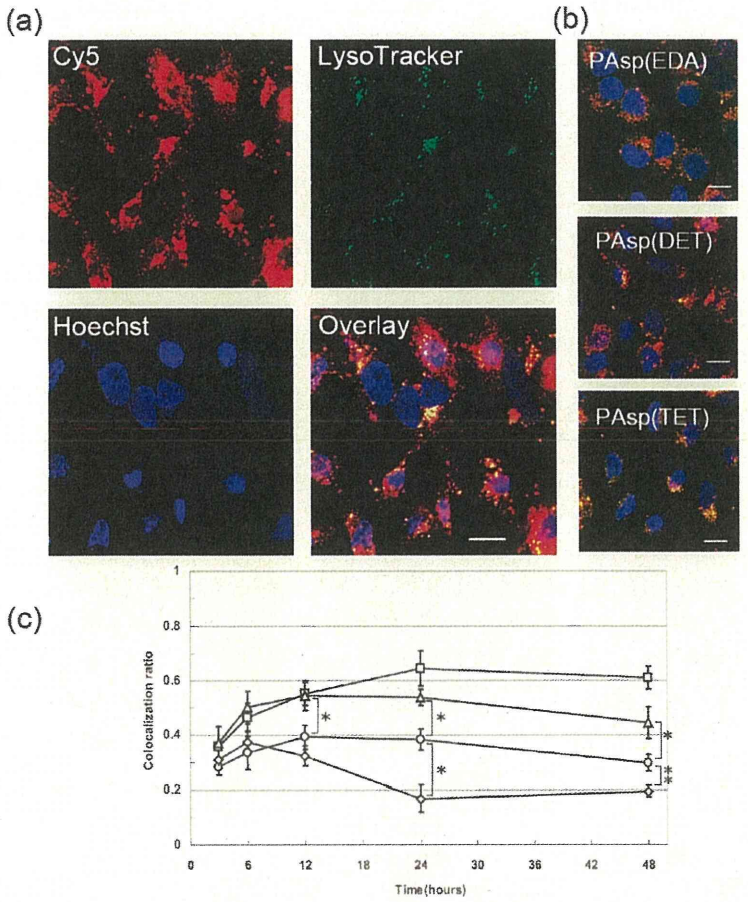

Figure 8. (a) Intracellular distribution of Cy5-labeled pDNA (red) complexed with PAsp(TEP) at N/P = 10 for Huh-7 cells after 48 h incubation. Acidic late endosomes and lysosomes were stained with LysoTracker Green (green). The nuclei were stained with Hoechst 33342 (blue). The scale bar represents 20 μm. (b) Overlay images of Cy5-labeled pDNA, LysoTracker Green, and Hoechst 33342 in Huh-7 transfected with the polyplexes from PAsp(EDA), PAsp(DET), and PAsp(TET) observed under the same conditions as those of part a. (c) Time-dependent changes in colocalization ratios of the PAsp(EDA) (square), PAsp(DET) (circle), PAsp(TET) (triangle), and PAsp(TEP) (diamond) polyplexes containing Cy5-labeled pDNA with late endosomes and lysosomes. Results are expressed as mean ± SEM (N = 10). *P < 0.05, **P < 0.01.

N-substituted polyaspartamides and the endosomal escape efficiency of their polyplexes. The buffering capacity was estimated from the change in the degree of protonation between pH 7.4 and 5.5 ($\Delta\alpha$) (Table 1) and was consistent with the observed odd−even effect. PA-Es [$\Delta\alpha$ = 0.31 and 0.19 for PAsp(DET) and PAsp(TEP), respectively] possess higher buffering capacities than PA-Os [$\Delta\alpha$ = 0.06 and 0.11 for PAsp(EDA) and PAsp(TET), respectively]. The assumed protonated structures of the side chains for each polymer (Figure 3) are rather interesting. Almost all the amino groups in the PAsp(EDA) side chains are protonated, regardless of pH (7.4 or 5.5). On the other hand, most of the PAsp(DET) side chains are in the monoprotonated state at pH 7.4 (α = 0.51) and diprotonated state at pH 5.5 (α = 0.82) owing to the appreciable difference in pK_{a_1} (8.9) and pK_{a_2} (6.2), as reported in our previous paper.[26] Low pK_{a_2} values in PAsp(DET) are due to the thermodynamic disadvantages of the diprotonated structure in 1,2-diaminoethane caused by electrostatic repulsion between the two protonated amines, locking the conformation in the *anti* form with less rotational freedom (butane effect). The absence of a significant change in α for PAsp(TET) with pH ($\Delta\alpha$ = 0.11) may be explained in a similar way: the fully protonated (triprotonated) structure of an *N*-(2-aminoethyl)-1,2-diaminoethane unit has a substantial thermodynamic penalty because of the strong repulsive force from the two neighboring protonated amines. Consequently, the side chain prefers to exist as a diprotonated structure with diethyleneamine spacing ($-NH_2^+-CH_2-CH_2-NH-CH_2-CH_2-NH_3^+$) containing a nonprotonated amino group in the center even at lower pH. Alternatively, for PAsp(TEP), α increases from 0.49 to 0.68 with a decrease in pH from 7.4 to 5.5 because the pK_{a_3} value (6.3) exists between these two pH values. As shown in Figure 3, the dominant structure changes from a diprotonated state at pH 7.4 to a triprotonated state at pH 5.5. The latter form, with its integrated positive charge, is still allowed under acidic conditions possibly because the increase in electrostatic repulsion accompanying the third protonation may be alleviated by sufficient length and rotational flexibility of the diethyeleneamine spacing ($-CH_2CH_2NHCH_2CH_2-$). Note that pK_{a_4} of PAsp(TEP) is much lower than the titration range (pH < 1.2) because of the highly repulsive nature of the fully protonated structure.

Although the buffering capacity may explain the odd−even effect observed in the transfection efficiency of the examined

polyplexes, it does not completely agree with the order of their endosomal escape efficiency. PAsp(DET) possessed relatively larger $\Delta\alpha$ than PAsp(TEP); however, the polyplex from the latter achieved significantly higher endosomal escape efficiency (lower endosomal colocalization ratio) than that from the former (Figure 8), suggesting the presence of an additional factor affecting the endosomal escape behavior of the polyplexes. In this regard, membrane destabilization directly by polycation interaction should be emphasized, as indicated from the result of the hemolysis assay shown in Figure 4. The odd−even effect was clearly observed in this assay and only the PA-E series induced a substantial increase in hemolysis at acidic pH. PAsp(TEP) demonstrated the highest hemolysis (14.4%), followed by PAsp(DET) (8.0%), PAsp(TET) (4.9%), and PAsp(EDA) (1.8%). The order of hemolytic activity at pH 5.5 agrees well with the endosomal escape efficiency of the polyplexes (Figure 8), suggesting that disturbing the membrane integrity may be important for the endosomal escape of these polyplexes. Furthermore, the weak hemolytic activity for each polymer at pH 7.4 agrees with their low cytotoxicity (Figure 6), suggesting their limited interaction with plasma membranes of mammalian cells under physiological conditions. Note that ExGen 500 also showed the membrane destabilizing activity in response to the acidic pH in the endosome (Figure 4). Nevertheless, it is assumed that the considerably high hemolytic activity (approximately 30%) of ExGen 500 at pH 7.4 may be correlated with its high cytotoxicity (Figure 6), suggesting that the augmentation of repeating aminoethylene units might increase cytotoxicity regardless of pH.

To further discuss the mechanism for cellular membrane destabilization induced by the N-substituted polyaspartamides, we focus here on the number of protonated amines (NA) and the overall cationic charge density (CD) in each polymer strand (Table 1). A previous study revealed that polycations with larger NA and higher CD tend to induce stronger disturbances in the membrane integrity, presumably resulting from a higher affinity of the plasma membrane for positively charged components.[33] Yet the calculated NA and CD were apparently not correlated with the hemolytic activity and simply increased with the number of aminoethylene units without any odd−even effects.

Next, we investigated whether the protonation state of the N-substituted polyaspartamides (Figure 3) would contribute to the odd−even effect from the viewpoint of specific interactions that may lead to a disturbance in the membrane integrity. It is interesting to consider that PA-Es [PAsp(DET) and PAsp(TEP), Figure 3] at pH 5.5 contain a diprotonated state of the diaminoethane unit ($-NH_2^+-CH_2-CH_2-NH_2^+-$), corresponding to their strong hemolytic activity in acidic conditions. In contrast, no such structure is determined for PA-Os [PAsp(EDA) and PAsp(TET)] at either pH 7.4 nor 5.5 nor for PA-Es at pH 7.4, and eventually they have very limited hemolytic activity. In particular, for PAsp(TET) at pH 7.4/5.5 and PAsp(TEP) at pH 7.4, two protonated amines are spatially separated by diethyleneamine ($-CH_2-CH_2-NH-CH_2-CH_2-$) or *N,N′*-ethylene-1,2-diaminoethane ($-CH_2-CH_2-NH-CH_2-CH_2-NH-CH_2-CH_2-$) spacers. It is likely that a critical spacing length between the two protonated amino groups may exist in order to induce an effective membrane interaction. Note that an N-substituted polyaspartamide possessing a 1,3-diaminopropane unit ($-NHCH_2CH_2CH_2NH-$) in the side chain [PAsp(DPT)] assumed a fully protonated structure at pH 7.4/5.5 and induced substantial membrane destabilization of mammalian cells, as previously reported.[26] It can be assumed that two positively charged units may need to be close to each other via a spacing equivalent of approximately two or three methylene units to exert a strong interaction with cellular membranes. The additional positively charged unit in the side chain of PAsp(TEP), separated from the diprotonated diamine unit ($-NH_2^+-CH_2-CH_2-NH_2^+-$) by a flexible $-CH_2-CH_2-NH-CH_2-CH_2-$ spacer, may contribute further to enhance the binding affinity through the formation of a polyvalent charged array as multiple binding sites. This multiple binding scheme reasonably explains PAsp(TEP) polyplex's higher hemolysis efficiency as well as its enhanced endosomal escape capability compared to that of PAsp(DET) polyplex, even though the former has a lower buffering capacity than the latter.

CONCLUSION

Efficient transfection without severe cytotoxicity was achieved by the polyplexes from the N-substituted polyaspartamides possessing the even-numbered repeating aminoethylene units in their side chains [PAsp(DET) and PAsp(TEP)]. This agrees with their appreciably high buffering capacity as well as their capability to disturb the membrane integrity selectively at endosomal pH, thereby facilitating the endosomal escape of the polyplexes. Results of the hemolysis assay and the CLSM observations tracking subcellular distribution of the polyplexes suggest that two protonated amino groups may need to be tethered with critical spacing equivalent to approximately two or three methylene units to induce the strong interaction of polycations in the polyplexes with the endosomal membrane, leading to their effective transport into the cytoplasm. Importantly, fine-tuning of the number, spacing, and protonation status of repetitive amine units in the polycation side chain, as reported in this study, resolves the conflict between endosomal escape and cytotoxicity of the polyplexes, thus providing a new design concept for nonviral gene delivery systems directed toward clinical applications.

ASSOCIATED CONTENT

Supporting Information. Experimental Section and supplemental Figures 1−3. This material is available free of charge via the Internet at: http://pubs.acs.org

AUTHOR INFORMATION

Corresponding Author
kataoka@bmw.t.u-tokyo.ac.jp

ACKNOWLEDGMENT

This work was financially supported in part by the Center for Medical System Innovation (CMSI) and the Funding Program for World-Leading Innovative R&D on Science and Technology (FIRST) from Japan Society for the Promotion of Science (JSPS) and the Core Research Program for Evolutional Science and Technology (CREST) from Japan Science and Technology Agency (JST). The authors thank Kotoe Date (The University of Tokyo) for her technical assistance.

REFERENCES

(1) Mastrobattista, E.; van der Aa, M. A.; Hennink, W. E.; Crommelin, D. J. A. *Nat. Rev. Drug Discovery* **2006**, *5*, 115–121.
(2) Mintzer, M. A.; Simanek, E. E. *Chem. Rev.* **2009**, *109*, 259–302.

(3) Pack, D. W.; Hoffman, A. S.; Pun, S. *Nat. Rev. Drug Discovery* **2005**, *4*, 581–593.
(4) Wood, K. C.; Little, S. R.; Langer, R.; Hammond, P. T. *Angew. Chem., Int. Ed.* **2005**, *44*, 6704–6708.
(5) Zugates, G. T.; Anderson, D. G.; Little, S. R.; Lawhorn, I. E. B.; Langer, R. *J. Am. Chem. Soc.* **2006**, *128*, 12726–12734.
(6) Srinivasachari, S.; Fichter, K. M.; Reineke, T. M. *J. Am. Chem. Soc.* **2008**, *130*, 4618–4627.
(7) Green, J. J.; Langer, R.; Anderson, D. G. *Acc. Chem. Res.* **2008**, *41*, 749–759.
(8) Schaffert, D.; Troiber, C.; Salcher, E. E.; Frohlich, T.; Martin, I.; Badgujar, N.; Dohmen, C.; Edinger, D.; Klager, R.; Maiwald, G.; Farkasova, K.; Seeber, S.; Jahn-Hofmann, K.; Hadwiger, P.; Wagner, E. *Angew. Chem., Int. Ed.* **2011**, *50*, 1–4.
(9) Wattiaux, R.; Laurent, N.; Coninck, W. N.; Jadot, M. *Adv. Drug Delivery Rev.* **2000**, *41*, 201–208.
(10) Wagner, E.; Plank, C.; Zatloukal, K.; Cotton, M.; Birnstiel, M. L. *Proc. Natl. Acad. Sci. U. S. A.* **1992**, *89*, 7934–7938.
(11) Haensler, J.; Szoka, F. C. *Bioconjugate Chem.* **1993**, *4*, 372–379.
(12) Boussif, O.; Lezoualc'h, F.; Zanta, M. A.; Mergny, M. D.; Scherman, D.; Demeneix, B.; Behr, J. P. *Proc. Natl. Acad. Sci. U. S. A.* **1995**, *92*, 7297–7301.
(13) Midoux, P.; Monsigny, M. *Bioconjugate Chem.* **1999**, *10*, 406–411.
(14) Thomas, M.; Kilbanov, A. M. *Proc. Natl. Acad. Sci. U. S. A.* **2002**, *99*, 14640–14645.
(15) Kwon, E. J.; Bergen, J. M.; Pun, S. H. *Bioconjugate Chem.* **2008**, *19*, 920–927.
(16) Hunter, A. C. *Adv. Drug Delivery Rev.* **2006**, *58*, 1523–1531.
(17) Neu, M.; Fischer, D.; Kissel, T. *J. Gene Med.* **2005**, *7*, 992–1009.
(18) Ferrari, S.; Moro, E.; Pettenazzo, A.; Behr, J. P.; Zacchello, F.; Scarpa, M. *Gene Ther.* **1997**, *4*, 1100–1106.
(19) Wightman, L.; Kircheis, R.; Rossler, V.; Carotta, S.; Ruzicka, R.; Kursa, M.; Wagner, E. *J. Gene Med.* **2001**, *3*, 362–372.
(20) Itaka, K.; Harada, A.; Yamasaki, Y.; Nakamura, K.; Kawaguchi, H.; Kataoka, K. *J. Gene Med.* **2004**, *6*, 76–84.
(21) Densmore, C. L.; Kleinerman, E. S.; Gautam, S.; Jia, S. F.; Xu, B.; Worth, L, L.; Waldrep, J. C.; Fung, Y. K.; Ang, A, T.; Knight, V. *Cancer Gene Ther.* **2001**, *8*, 619–627.
(22) Smits, R. G.; Koper, G. J. M.; Mandel, M. *J. Phys. Chem.* **1993**, *97*, 5745–5751.
(23) Merdan, T.; Kunath, K.; Fischer, D.; Kopecek, J.; Kissel, T. *Pharm. Res.* **2002**, *19*, 140–146.
(24) Bieber, T.; Meissener, W.; Kostin, S.; Niemann, A.; Elsasser, H.-P. *J. Controlled Release* **2002**, *82*, 441–454.
(25) Walker, G. F.; Fella, C.; Pelisek, J.; Fahrmeir, J.; Boeckle, S.; Ogris, M.; Wagner, E. *Mol. Ther.* **2005**, *11*, 418–425.
(26) Miyata, K.; Oba, M.; Nakanishi, M.; Fukushima, S.; Yamasaki, Y.; Koyama, H.; Nishiyama, N.; Kataoka, K. *J. Am. Chem. Soc.* **2008**, *130*, 16287–16294.
(27) Moghimi, S. M.; Symonds, P.; Murray, J. C.; Hunter, A. C.; Debska, G.; Szewczk, A. *Mol. Ther.* **2005**, *11*, 990–995.
(28) Kanayama, N.; Fukushima, S.; Nishiyama, N.; Itaka, K.; Jang, W. D.; Miyata, K.; Yamasaki, Y.; Chung, U.; Kataoka, K. *ChemMedChem.* **2006**, *1*, 439–444.
(29) Itaka, K.; Ohaba, S.; Miyata, K.; Kawaguchi, H.; Nakamura, K.; Takato, T.; Chung, U.; Kataoka, K. *Mol. Ther.* **2007**, *15*, 1655–1662.
(30) Harada-Shiba, M.; Takamisawa, I.; Miyata, K.; Ishii, T.; Nishiyama, N.; Itaka, K.; Kangawa, K.; Yoshihara, F.; Asada, Y.; Hatakeyama, K.; Nagaya, N.; Kataoka, K. *Mol. Ther.* **2009**, *17*, 1180–1186.
(31) Arnida; Nishiyama, N.; Kanayama, N.; Jang, W.-D.; Yamasaki, Y.; Kataoka, K. *J. Controlled Release* **2006**, *115*, 208–215.
(32) Nakanishi, M.; Park, J.-S.; Jang, W.-D.; Oba, M.; Kataoka, K. *React. Funct. Polym.* **2007**, *67*, 1361–1372.
(33) Fisher, D.; Li, Y.; Ahlemeyer, B.; Kreglstein, J.; Kissel, T. *Biomaterials* **2003**, *24*, 1121–1131.

Biomacromolecules

ARTICLE

pubs.acs.org/Biomac

Effect of Polymer Structure on Micelles Formed between siRNA and Cationic Block Copolymer Comprising Thiols and Amidines

R. James Christie,[†] Kanjiro Miyata,[‡,§,∥] Yu Matsumoto,[‡,⊥,#] Takahiro Nomoto,[∥] Daniel Menasco,[○] Tzai Chung Lai,[○] Matthew Pennisi,[†] Kensuke Osada,[†,§] Shigeto Fukushima,[†] Nobuhiro Nishiyama,[‡] Yuichi Yamasaki,[†,§] and Kazunori Kataoka*[,†,‡,§,∥]

[†]Department of Materials Engineering, Graduate School of Engineering, The University of Tokyo, Japan

[‡]Division of Clinical Biotechnology, Center for Disease Biology and Integrative Medicine, Graduate School of Medicine, The University of Tokyo, Japan

[§]Center for NanoBio Integration, The University of Tokyo, Japan

[∥]Department of Bioengineering, Graduate School of Engineering, The University of Tokyo, Japan

[⊥]Department of Otorhinolaryngology and Head and Neck Surgery, Graduate School of Medicine and Faculty of Medicine, The University of Tokyo, Japan

[#]Department of Otorhinolaryngology and Head and Neck Surgery, Mitsui Memorial Hospital, Japan

[○]Center for Medical Systems Innovation Summer Internship Program, The University of Tokyo, Japan

Supporting Information

ABSTRACT: Small interfering RNA (siRNA) has great therapeutic potential for the suppression of proteins associated with disease, but delivery methods are needed for improved efficacy. Here, we investigated the properties of micellar siRNA delivery vehicles prepared with poly(ethylene glycol)-*block*-poly(L-lysine) (PEG-*b*-PLL) comprising lysine amines modified to contain amidine and thiol functionality. Lysine modification was achieved using 2-iminothiolane (2-IT) [yielding PEG-*b*-PLL(N2IM-IM)] or dimethyl 3,3′-dithiobispropionimidate (DTBP) [yielding PEG-*b*-PLL(MPA)], with modifications aimed to impart disulfide cross-linking ability without compromising cationic charge. These two lysine modification reagents resulted in vastly different chemistry contained in the reacted block copolymer, which affected micelle formation behavior and stability along with in vitro and in vivo performance. Amidines formed with 2-IT were unstable and rearranged into a noncharged ring structure lacking free thiol functionality, whereas amidines generated with DTBP were stable. Micelles formed with siRNA and PEG-*b*-PLL(N2IM-IM) at higher molar ratios of polymer/siRNA, while PEG-*b*-PLL(MPA) produced micelles only near stoichiometric molar ratios. In vitro gene silencing was highest for PEG-*b*-PLL(MPA)/siRNA micelles, which were also more sensitive to disruption under disulfide-reducing conditions. Blood circulation was most improved for PEG-*b*-PLL(N2IM-IM)/siRNA micelles, with a circulation half-life 3× longer than naked siRNA. Both micelle formulations are promising for siRNA delivery applications in vitro and in vivo.

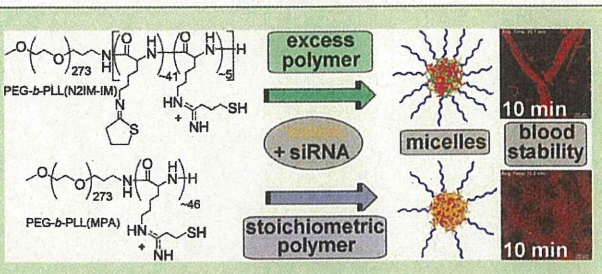

INTRODUCTION

Small interfering ribonucleic acid (siRNA) is capable of sequence-specific gene silencing without altering the host genome, a property that could be exploited to suppress proteins associated with disease. Thus, there is a strong impetus for development of practical, safe, and effective siRNA-based therapies. However, the inherent properties of siRNA molecules such as large size, anionic nature, and susceptibility to degradation preclude direct use for treatment of disease. Many clever materials have been developed that encapsulate siRNA until the intracellular site of activity is reached to improve its therapeutic activity. Structures formed after encapsulation of siRNA are often referred to as "siRNA carriers" or "siRNA delivery systems". To date, the types of materials explored as siRNA carriers include cationic lipids, cyclodextrins, branched and linear polycations, cationic block copolymers, and various peptides. General siRNA delivery strategies and considerations for the design of appropriate carriers have recently been reviewed.[1,2]

Polyion complexes (PICs) are often used to bind and encapsulate siRNA by exploiting its anionic nature.[3] PIC formation is a widely used strategy for preparation of advanced materials

Received: May 17, 2011
Revised: July 2, 2011
Published: August 24, 2011

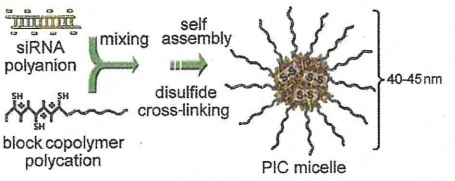

Figure 1. Preparation of disulfide cross-linked PIC micelles containing siRNA.

and diagnostics in the field of biomedical technology. PIC-based materials form by electrostatic attraction of oppositely charged polymers, with the release of water solvating charged functional groups providing further energetic gain. These functional materials may exploit single pairs of polyelectrolytes or multiple layering of charged polymers, with polyions from both natural and synthetic origin commonly used. The general strategy of PIC formation has been applied to prepare drug delivery systems, capture analytes for sensors, and form surface coatings, in addition to the formation of polyplexes with nucleic acids as described here.[4−7] PIC formation between nucleic acids and polycations generally results in nanosized structures with morphologies ranging from spheres to rods.[8] Furthermore, advanced PIC-based nucleic acid carriers have been engineered to contain "smart" properties such as PEG palisades to reduce nonspecific interactions with biological components, targeting ligands for tissue-specific accumulation, and also mechanisms for site-specific cargo release through environment-sensitive chemistries.[9−13]

Recently, we reported a PIC micelle siRNA delivery system prepared from the block copolymer poly(ethylene glycol)-*block*-poly(L-lysine) (PEG-*b*-PLL) modified with the cross-linking reagent 2-iminothiolane (2-IT, Traut's reagent).[14] The resulting block copolymer, termed PEG-*b*-PLL(IM), was designed to contain cationic amidine groups for PIC formation with anionic siRNAs and also free sulfhydryls to allow disulfide cross-linking in the micelle core for improved stability. Covalent disulfide cross-links are particularly attractive for micelle core stabilization because they are reversible and more susceptible to cleavage (reduction) at the subcellular site of activity where the levels of natural disulfide reducing agents are higher than in the bloodstream.[15] Disulfide cross-linked PIC micelle formation between siRNA and thiol-modified cationic block copolymer is shown in Figure 1.

Modification of PEG-*b*-PLL with 2-IT improved the quality of the resulting micelles (controlled size and PDI), increased micelle stability, and enhanced siRNA activity in vitro. However, micelles formed only at specific molar ratios of polymer/siRNA, and this optimal ratio increased with increased IM content in the PLL block. One possible explanation for this observed complexation behavior between PEG-*b*-PLL(IM) and siRNA could be related to the instability of amidines formed with 2-iminothiolane. Rearrangement of 2-IT modified amines is known to occur following reaction with amino acids and involves intramolecular reaction of sulfur with the amidine carbon, subsequent release of ammonia, and formation of a N-substituted 2-iminothiolane ring. This five-membered ring structure contains an imine bond ($pK_a \sim 6.7$) not an amidine ($pK_a \sim 12$), thus, reducing the positive charge of the block copolymer at pH 7.4.[16,17]

The focus of this work was to better understand the micelle formation behavior between PEG-*b*-PLL(IM) and siRNA, with the hypothesis that formation of N-substituted 2-iminothiolanes affects the formation and properties of micelles. This was accomplished by comparing 2-IT with the analogous amine-reactive amidination reagent, dimethyl 3,3′-dithiobispropionimidate (DTBP), to yield PEG-*b*-PLL(MPA). DTBP differs from 2-IT by a methylene unit between the thiol and amidine functional group, which prevents formation of N-substituted 2-iminothiolane ring structures due to the instability of a 4-membered ring. Comparison between the two polymer analogues clarified the siRNA complexation behavior previously observed for PEG-*b*-PLL(IM) and also provided insight into the structure−function relationship between the block copolymer component and the properties of resulting micelle structures. Micelle formulations prepared from both block copolymers represent improvements compared to naked siRNA and noncross-linked PICs, and are promising candidates for further development.

In this study we directly observed both N-substituted 2-iminothiolane rings and also linear 1-(4-mercaptobutyl) amidine groups upon ^{1}H NMR analysis of the reaction product of PEG-*b*-PLL with 2-IT, and have named the polymer "PEG-*b*-PLL-(N2IM-IM)".

EXPERIMENTAL SECTION

General. *N*-Methyl-2-pyrrolidinone (NMP, 99.5% anhydrous), LiCl (>99%), sodium tetraborate decahydrate (99.5%), diisopropylethylamine (DIPEA, 99.5%), 2N HCl solution, D_2O (99.9%), tetramethylsilane (TMS, 99.5%), and DCl (35% in D_2O) were obtained from Sigma Aldrich (St. Louis, MO) and used without further purification. 2-Iminothiolane hydrochloride (2-IT), diethyl ether (99+%), dithiothreitol (DTT, molecular biology grade DNase and RNase free), ethylenediamine tetraacetic acid disodium salt dihydrate (EDTA, 99.5%), sodium bicarbonate (99.5−100.3%), sodium dihydrogen phosphate·$2H_2O$ (99−102%), disodium hydrogen phosphate·$12H_2O$ (99+%), glutathione (reduced form), and sodium chloride (99+%) were supplied by Wako Pure Chemical Industries (Osaka, Japan). Dimethyl 3,3′-dithiobispropionimidate·2HCl (DTBP), Ellman's reagent [5,5-dithiobis-(2-nitrobenzoic acid)], 2,4,6-trinitrobenzene sulfonic acid (5% w/v in methanol), and slide-a-lyzer dialysis cassettes (MWCO = 3.5 kDa) were obtained from Thermo Scientific (Rockford IL). Sterile HEPES (1 M, pH 7.3) was purchased from Amresco (Solon, OH). Spectra/Por dialysis tubing (10 KDa MWCO) was acquired from Spectrum Laboratories (Rancho Dominguez, CA). Firefly GL3 luciferase siRNA (sense: 5′-CUU ACG CUG AGU ACU UCG AdTdT-3′; antisense: 5′-UCG AAG UAC UCA GCG UAA GdTdT-3′) Cy3-labeled firefly luciferase siRNA, Cy5-labeled firefly luciferase siRNA, and scramble siRNA (sense: 5′-UUC UCC GAA CGU GUC ACG UdTdT-3′; antisense: 5′-ACG UGA CAG GUU CGG AGA AdTdT-3′) were synthesized by Hokkaido System Science Co., Ltd. (Hokkaido, Japan) with dye labels attached to the sense strands.

^{1}H NMR analysis of PEG-*b*-PLL(N2IM-IM) was conducted in D_2O containing 0.05% v/v tetramethylsilane and 3 μL/mL DCl solution (35% DCl in D_2O) at 22 °C using a 300 MHz spectrometer (EX 300, JEOL, Tokyo, Japan). ^{1}H NMR analysis of PEG-*b*-PLL(MPA) and PEG-*b*-PLL was conducted in the same fashion as PEG-*b*-PLL(N2IM-IM) except without DCl.

Static and dynamic light scattering measurements were performed at 25 °C on a ZetaSizer Nano ZS instrument (Malvern Instruments Ltd., Malvern, U.K.) equipped with a He−Ne laser (λ = 633 nm) as the incident beam with samples (16 μL) loaded into a Zen 2112 low-volume cuvette. Absorbance and fluorescence measurements were performed with NanoDrop ND-1000 and ND-3300 instruments (NanoDrop Technologies Inc., Rockland DE), respectively.

Scheme 1. Synthesis of PEG-*b*-PLL Derivatives

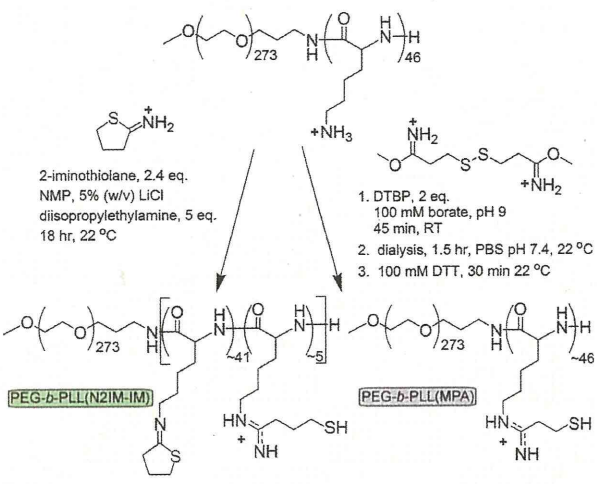

The luciferase-expressing mouse melanoma cancer cell line, B16F10-luc, was purchased from Caliper LifeScience (Hopkinton, MA). Dulbecco's modified eagle's medium (DMEM) was obtained from Sigma Aldrich (St. Louis, MO). Fetal bovine serum was provided by Dainippon Sumitomo Pharma Co. (Osaka, Japan). Falcon Easy-Grip 35 × 10 mm vacuum gas plasma-treated polystyrene tissue culture dishes were obtained from BD Biosciences (San Jose, CA). Luciferin was purchased from Summit Pharmaceutical International (Tokyo, Japan). Luciferase bioluminescence in B16F10-luc cells was measured using an ATTO Kronos Dio photon countable incubator (ATTO Corp., Tokyo, Japan).

Synthesis of PEG-*b*-PLL(N2IM-IM). PEG-*b*-PLL copolymer was synthesized as previously described, comprising a 12000 MW PEG segment and a 45 amino acid PLL segment.[13,18] Iminothiolane modification of PEG-*b*-PLL was achieved by reacting primary amino groups contained in the side chains of PLL with 2-IT, as outlined in Scheme 1. First, 50 mg PEG-*b*-PLL (0.12 mmol amine, 1 equiv) was added to 2 mL NMP containing 5 wt % LiCl and the reaction vessel was purged with Ar and then capped with a septum. The polymer solution was placed into an oil bath at 50 °C and stirred for 30 min to completely dissolve all solids. After dissolution of polymer, the solution was removed from heat and cooled to 22 °C. Next, DIPEA (100 μL, 1.1 mmol, 5 equiv relative to Lys amines) was added to the polymer solution under Ar through the septum. Finally, 2-iminothiolane·HCl (39 mg, 0.28 mmol, 2.4 equiv relative to lysine amines) was added directly to the polymer solution. The reaction continued with stirring for 18 h at 22 °C under an argon atmosphere. After 18 h, the reaction was terminated by precipitation into a 10× volume excess of dry diethyl ether. Precipitated product was washed several times with ether and dried under vacuum to a constant mass. Crude product was redissolved in PBS buffer (10 mM phosphate, 150 mM NaCl, pH 6.0) and then dialyzed (SpectraPor7, 10 kDa MWCO) against PBS pH 6.0 for one day and distilled water for one day with frequent media changes. Dialyzed polymer solution was passed through a 0.2 μM filter and then lyophilized. Yield: 55 mg (96%), white powder. The degree of lysine modification was determined from the ^{1}H NMR spectra recorded in acidic D_2O (Figure 2) by the peak intensity ratio of the β, γ, and δ-methylene protons of Lys ($(CH_2)_3$, δ = 1.3–1.9 ppm) to the sum of peak intensities of methylene protons from the C4 carbon of N-substituted 2-iminothiolane groups and the protons of trimethylene units of mercaptopropyl groups (HS-$(CH_2)_3$, δ = 2.1, 2.6, and 2.8 ppm). The calculated IM introduction rate was 95%. The ratio of 1-(4-mercaptobutyl) amidine groups to N-substituted 2-iminothiolane groups was determined by the peak intensity ratios of methylene protons from the C4 position on N-substituted 2-iminothiolane groups (2.4 ppm) and protons of trimethylene units of mercaptopropyl groups (HS-$(CH_2)_3$, δ = 2.1, 2.6, and 2.8 ppm). The ratio of 1-(4-mercaptobutyl) amidine to N-substituted 2-iminothiolane was ~0.25.

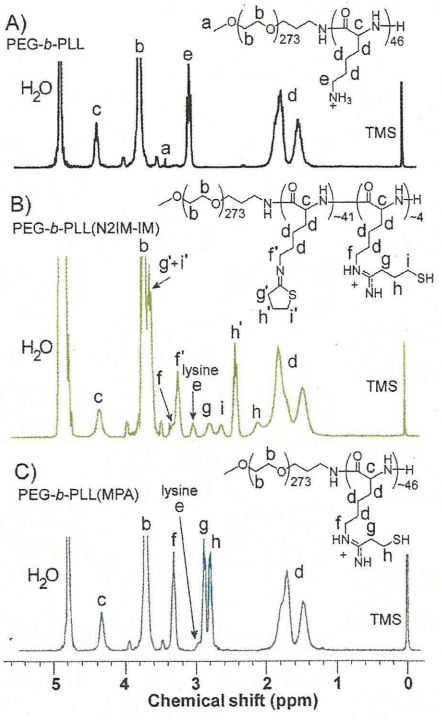

Figure 2. ^{1}H NMR spectra of PEG-*b*-PLL and modification products. Spectra were recorded at 300 mHz, 25 °C in D_2O (A,C) or D_2O containing 3 μL/mL 35% DCl solution (B). Residual lysine residues are not included in the chemical structures shown in (B) and (C).

Synthesis of PEG-*b*-PLL(MPA). PEG-*b*-PLL(MPA) was synthesized by reaction of lysine primary amines with amido esters contained in DTBP as shown in Scheme 1. First, PEG-*b*-PLL (300 mg, 0.7 mmol amines, 1 equiv) of the same parent stock used for synthesis of PEG-*b*-PLL(N2IM-IM) was dissolved in 100 mM sodium borate, pH 9.0 (60 mL) and then DTBP·HCl (439 mg, 1.4 mmol, 2 equiv relative to lysine amines) was added to the polymer solution. The reaction was stirred at room temperature for 45 min and then transferred to slide-a-lyzer dialysis cassettes (MWCO 3500) and dialyzed against PBS (10 mM phosphate, 150 mM NaCl, pH 7.4) for 1.5 h to remove unreacted DTBP. The reaction mixture was recovered and then DTT (300 mg) was added to generate the free sulfhydryl in polymer-reacted DTBP. The reaction was stirred at room temperature for 30 min and then transferred to slide-a-lyzer dialysis cassettes (MWCO 3500). Dialysis was performed against 10 mM PBS, pH 6.0 for 2 h and then distilled water for 2 h with rapid stirring and frequent exchange of dialysis media. The purified polymer solution was passed through a 0.2 μm filter and lyophilized. Yield: 299 mg (73%), white powder. The degree of DTBP introduction was determined from the ^{1}H NMR spectra shown in Figure 2 by the peak intensity ratio of the β, γ, and δ-methylene protons of Lys ($(CH_2)_3$, δ = 1.3–1.9 ppm) to the protons of mercaptoethyl groups (HS-$(CH_2)_2$, δ = 2.7–2.9 ppm). The calculated degree of lysine modification was 95%.

Analysis of Thiol Content in Block Copolymers. Free thiol content in modified block copolymers was determined by Ellman's assay.[19] Polymer solutions (5 mg/mL) were incubated in 10 mM HEPES buffer containing 5 mM EDTA and 15 mM DTT for 30 min

Table 1. Summary of Polymer and Micelle Properties

	PEG-*b*-PLL[l]	PEG-*b*-PLL(N2IM-IM)	PEG-*b*-PLL(MPA)
MW[a]	19600	22000	23350
% modified lysines[b]	0	95	95
% thiol content[c]	0.7 ± 0.04	11 ± 2.5	90 ± 12
polymer/siRNA molar ratio with maximum SLI at pH 7.4/5.0[d]	1.2/ND	≥7.6/1.4	1.2/1.3
micelle size (d.nm)[e,f,g]	194 ± 15	42.4 ± 2.2	41.8 ± 2.1
micelle PDI[e,g]	0.44 ± 0.1	0.07 ± 0.02	0.05 ± 0.02
micelle ζ potential[g]	ND	−1.99 ± 0.47	−0.50 ± 1.26
micelle stability in 600 mM NaCl[d,g,h]	<5%	86%	43%
% remaining thiol in cross-linked micelles[c,i]	ND	52 ± 0.54	3.7 ± 0.27
maximum gene silencing[g,j]	<5%	~12%	~40%
circulation half-life[g,k]	~ 3 min	~10 min	~6 min

[a] Including chloride counterion. [b] Determined by ^{1}H NMR. [c] Determined by Ellman's Assay. [d] Determined by static light scattering, 25 °C. [e] Determined by dynamic light scattering, pH 7.4, 25 °C. [f] Reported as the *z*-average cumulant mean diameter. [g] Cross-linked micelles prepared at the polymer/siRNA molar ratio of max SLI. [h] Stability relative to cross-linked micelles in 10 mM HEPES, pH 7.4. [i] Expressed relative to the free thiol content measured in polymer before micelle formation. [j] Determined in B16F10-luc cancer cells, 200 nM siRNA, 48 h. [k] Determined by in vivo confocal intravital microvideography, 24 μg siRNA injection. [l] Structures formed with siRNA may not be micelles due to their large size and PDI.

at room temperature to reduce any disulfides present. The reduced polymer solution was placed on ice and handled in a timely manner at 0−4 °C until the addition of Ellman's reagent. After reduction, DTT was removed from the polymer solution using a NanoSep centrifugation device (3000 MWCO). Samples were subjected to three successive concentration/rinsing cycles with 10 mM HEPES containing 5 mM EDTA as the rinsing buffer. After the final centrifugation cycle, concentrated polymer solution was collected and diluted to its original volume. The final flow-through fraction was also collected and diluted in the same manner as the polymer-containing fraction to determine the amount of DTT remaining in the sample. Polymer and flow through samples were subjected to Ellman's assay according to the manufacturers protocol and sample absorbance was measured at 412 nm. Free thiol content of solutions was determined from a standard curve generated with reduced glutathione, and the thiol content in the polymer fraction was obtained by subtracting the thiol content in the flow-through fraction to correct for residual DTT. PEG-*b*-PLL was analyzed as a negative control in a similar fashion, except the polymer solution (5 mg/mL) was used directly without DTT incubation.

Complexation of Block Copolymers with siRNA. Block copolymer complexation and micelle formation with siRNA was studied as a function of the molar ratio of polymer/siRNA using the polymer molecular weights shown in Table 1. It should be noted that siRNA contains 40 negative charges and the poly(L-lysine) segment in the block copolymer contains ~46 units. Thus, if all modified PLL side-chains are charged the polymer/siRNA molar ratio and +/− charge ratio are nearly interchangeable. Polymer samples were dissolved in 10 mM HEPES buffer (pH 7.4) at a concentration of 5 mg/mL and aliquots were further diluted from this stock solution for preparation of complexation mixtures with siRNA. PEG-*b*-PLL(MPA) polymer solutions were diluted first with HEPES buffer to generate a solution twice the concentration desired for mixing with siRNA, and then 1:1 with HEPES buffer containing 30.54 mg/mL DTT. PEG-*b*-PLL(N2IM-IM) polymer solutions were reduced by direct addition of DTT to the 5 mg/mL polymer stock solution to yield 15.25 mg/mL DTT. Polymer solutions were incubated for 30 min at room temperature after addition of DTT to ensure cleavage of any disulfides present. Complexation was achieved by mixing polymer solution with siRNA (15 μM in 10 mM HEPES buffer, pH 7.4) at a volume ratio of 1:2 (polymer/siRNA) and PIC micelles were allowed to form for 24 h at 25 °C. For micelle formation at pH 5.0, both reduced polymer and siRNA solutions were acidified with appropriate volumes of 0.05 M HCl prior to mixing, then combined immediately. Disulfide cross-linked micelles were prepared by dialysis (slide-a-lyzer cassette (MWCO 3.5 kDa)) against 10 mM HEPES pH 7.4 containing 0.5% v/v DMSO for 2 days, followed by 2 days of dialysis against HEPES for removal of DMSO. DMSO was included in the dialysis buffer to assist in disulfide formation, as it is a mild oxidant specific toward thiols.[20] All disulfide cross-linked micelle samples were prepared at the polymer/siRNA molar ratio that exhibited maximum light scattering intensity in optimization experiments, polymer/siRNA = 7.6 for PEG-*b*-PLL(N2IM-IM) and 1.3 for PEG-*b*-PLL(MPA). Free thiol content in cross-linked micelles was determined using the Elman's assay according to the manufacturers protocol by sample absorbance at 412 nm and a standard curve generated with reduced glutathione. PEG-*b*-PLL(N2IM-IM) micelles were used directly for the assay whereas PEG-*b*-PLL(MPA)/siRNA micelles were concentrated 4-fold using NanoSep centrifugation devices (3000 MWCO) to yield a micelle solution with a theoretical thiol content within the range of the calibration curve.

Characterization of Micelles. PIC micelle solutions were analyzed by static and dynamic light scattering (DLS) to determine scattered light intensity (SLI) and PIC micelle size/PDI, respectively. Size distributions were determined by cumulant and histogram analysis of DLS data. Results are shown as the *z*-average diameter (cumulant mean) with the polydispersity index (PDI) (defined in the ISO standard document 13321:1996) and histogram of size distribution, as determined by the software provided by the manufacturer. The ζ-potentials of cross-linked PIC micelles prepared at the polymer/siRNA molar ratio with maximum SLI were measured in 10 mM HEPES buffer (pH 7.4) containing 150 mM NaCl at 37 °C. All samples were equilibrated to the defined temperature for 2 h prior to measurement. For fluorescence quenching experiments, PIC micelle solutions were prepared at various polymer/siRNA molar ratios as described above except Cy3-labeled GL3 siRNA was used. After 24 h incubation in the dark at 25 °C, the fluorescence intensity was measured with a NanoDrop ND-3300 instrument using white LED excitation.

In Vitro Stability of Micelles. Disulfide cross-linked PIC micelle stability was measured as a function of NaCl concentration in the presence or absence of the disulfide reducing agent DTT. Cross-linked micelle samples were diluted 1:1 with NaCl solution at desired concentrations and incubated at 37 °C for 24 h. Samples subjected to disulfide reducing conditions were diluted in the same fashion as above, however, with NaCl solutions containing 200 mM DTT. After the 24 h incubation period, samples were measured by static and dynamic light scattering, as described in the micelle characterization section.

TEM Analysis of Cross-Linked Micelles. Cross-linked micelle morphology was directly observed by transmission electron microscopy (TEM). For each analysis, the nucleic acid stain uranyl acetate (10 μL of a 2% w/v solution) was deposited onto a glass slide followed by sample solution (10 μL). This mixture was allowed to stand for 30 s in order to achieve effective staining. A carbon-coated 400 mesh Cu grid (Nisshin EM) was then immersed into the sample, allowing both sides of the grid to become fairly saturated. The grid was air-dried on a piece of filter paper and then transferred to a H-7000 TEM (Hitachi Ltd., Tokyo, Japan) for imaging. Images were recorded at optical magnifications of 50000 and 80000 with an acceleration voltage of 75 kV.

Micelle size distributions were determined from TEM images using ImageJ (available online at http://rsb.info.nih.gov/ij/download.html). TEM images previously modified by the addition of a scale bar were uploaded onto a computer and opened with ImageJ. A pixel to nanometer conversion value was generated by manually drawing a line on the scale bar and utilizing the program's built in Analyze → Set Scale command. Following creation of the pixel:nanometer conversion factor, lines were drawn by hand on each individual particle and their nanometer value was obtained via the Analyze → Measure command. A total of 46 particles were analyzed from each image. The raw data was imported into Microsoft Excel and histograms were generated.

In Vitro Gene Silencing. The gene silencing activity of siRNA incorporated in cross-linked micelles was determined in B16F10 murine melanoma cancer cells stably expressing luciferase (B16F10-luc), with luciferase targeted for gene knockdown. Cross-linked micelles containing GL3 (target) or scramble (off-target) siRNA were prepared as described above. Cells were cultured in Dulbecco's modified eagle's medium (DMEM) containing 10% fetal bovine serum (FBS). B16F10-luc cells were seeded onto 35 mm Petri dishes (25000 cells/dish) and allowed to attach for 24 h. After cell attachment, the media was removed and replaced with media (2 mL) containing 100 μM luciferin and cross-linked micelles corresponding to 200 nM micelle-encapsulated siRNA. For each analysis, control cell samples were prepared by addition of media diluted with HEPES instead of micelle solution. The total dilution of media after addition of luciferin and micelle solution was less than 200 μL additives per 10 mL of media. Samples were placed into a Kronos real-time photon-countable incubator and the luminescence intensity was measured periodically over a 55 h time period, with the temperature and CO_2 maintained at 37 °C and 5%. The amount of gene silencing was determined by dividing the average luminescence intensity of treated samples by the average luminescence intensity of control samples, $n = 4$.

In Vivo Micelle Stability. SiRNA incorporating micelle stability in the blood compartment was evaluated using intravital confocal videography in live mice. All picture/movie acquisitions were performed using a Nikon A1R confocal laser scanning microscope system attached to an upright ECLIPSE FN1 (Nikon Corp., Tokyo, Japan) equipped with a 20× objective, 640 nm diode laser, and a band-pass emission filter of 700/75 nm. The pinhole diameter was set to result in a 10 μm optical slice. Eight-week-old female BALB/c nude mice (Oriental Yeast Co., Ltd., Tokyo, Japan) were anesthetized with 2.0−3.0% isoflurane (Abbott Japan Co., Ltd., Tokyo, Japan) using a Univenter 400 Anaesthesia Unit (Univentor Ltd., Zejtun, Malta). Mice were then subjected to lateral tail vein catheterization with a 30-gauge needle (Becton, Dickinson and Co, Franklin Lakes, NJ, U.S.A.) connected to a nontoxic medical grade polyethylene tube (Natsume Seisakusho Co., Ltd., Tokyo, Japan). Anesthetized mice were placed onto a temperature-controlled pad (Thermoplate; Tokai Hit Co., Ltd., Shizuoka, Japan) integrated into the microscope stage and maintained in a sedated state throughout the measurement. Ear lobe dermis was observed without surgery and was easily fixed beneath a coverslip with a single drop of immersion oil. Data was acquired in video mode for 3 min (30 frames/sec), followed by snapshots every 1 min thereafter. All animal experimental procedures were performed in accordance with the Guide for the Care and Use of Laboratory Animals as stated by the National Institutes of Health.

Micelles prepared with Cy5-labeled siRNA at the polymer/siRNA molar ratio corresponding to maximum SLI (7.6 for PEG-*b*-PLL(N2IM-IM) and 1.2 for PEG-*b*-PLL(MPA)) were injected (200 μL of 9.2 μM siRNA, ~24 μg total siRNA) via the tail vein 10 s after the start of video capture. Micelles prepared with PEG-*b*-PLL(N2IM-IM) or PEG-*b*-PLL(MPA) and siRNA were cross-linked, as described above before injection.

Video data was analyzed by selecting regions of interest (ROIs) within blood vessels or extravascular skin tissue and the average fluorescence intensity per pixel for each time point was determined using the Nikon NIS-Elements C software provided by the manufacturer. To produce the blood retention profiles shown in Figure 6, vein fluorescence data was expressed relative to the maximum observed value. First, the background fluorescence intensity was determined from video captured during the 10 s before sample injection. This background value was then subtracted from the average pixel intensities measured after micelle injection to create background-corrected intensities for each time point. Next, relative fluorescence intensities were determined by dividing the average fluorescence intensity at each time point by the maximum observed fluorescence intensity (typically observed ~1 min). Analysis of tissue fluorescence intensity was performed in the same manner, without normalizing to the maximum observed value. Each experiment was performed in duplicate in separate animals, with representative data from a single animal shown in Figure 6. Individual circulation data for each mouse is provided as Supporting Information. A detailed description of the microscope apparatus and mouse positioning for intravital confocal micro videography, as well as examples of data workup showing ROIs can be found in our previously published report.[21]

RESULTS

Modification of PEG-*b*-PLL with 2-IT. PEG-*b*-PLL was reacted with excess 2-IT under organic conditions, as previously described, except 2-IT was added directly to the reaction mixture as a solid instead of dropwise addition of a solution.[14] The reaction proceeded by nucleophilic attack of lysine amine groups on the imine carbon contained in 2-IT, followed by ring-opening and generation of the free sulfhydryl (which may subsequently react with the amidine carbon as discussed below). Analysis of the PEG-*b*-PLL(N2IM-IM) polymer product by ^{1}H NMR spectroscopy showed that the desired modification was successful, as the lysine ε-CH_2 peak was shifted downfield and methylene peaks corresponding to N2IM and IM groups appeared in the spectrum (Figure 2). Both linear 1-(4-mercaptobutyl) amidine and cyclic N-substituted 2-iminothiolane groups were observed in the product, with the majority of side chains (~75%) being in the closed ring form based on integration values. Nearly complete conversion (95%) of lysine amine groups was achieved by this synthesis procedure. It should be noted that 2 mol equiv of 2-IT (relative to lysine amines) is necessary to achieve nearly complete modification of lysine amines. Addition of 1 mol equiv of 2-IT resulted in only ~60% conversion of lysine amines (data not shown).

2-IT modified polymer product was soluble in buffer despite the loss of charged functional groups. However, polymer self-association at 10 mg/mL interfered with ^{1}H NMR analysis in D_2O and acidification of the sample greatly clarified the spectrum. PEG-*b*-PLL(N2IM-IM) polymer solution showed very little light scattering at the concentration used for siRNA complexation (1.67 mg/mL) and addition of siRNA to the polymer

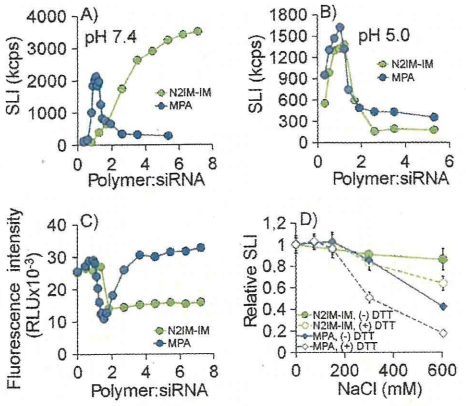

Figure 3. Light scattering behavior of siRNA and PEG-*b*-PLL(X) (*X* = N2IM-IM or MPA) mixtures, fluorescence quenching, and the stability of resulting cross-linked micelles. (A) Complexation of block copolymers with siRNA at pH 7.4, 25 °C. (B) Complexation of block copolymers with siRNA at pH 5.0, 25 °C. (C) Fluorescence quenching of Cy3-siRNA/block copolymer mixtures at pH 7.4, 25 °C. (D) Stability of disulfide cross-linked micelles following 24 h incubation at 37 °C in NaCl solutions with or without disulfide reducing agent (DTT). Data represents the average value ± standard deviation, $n = 3$. All polymer/siRNA ratios are molar ratios.

solution resulted in a 10-fold increase in scattered light intensity. A detailed analysis of polymer solution light scattering at pH 7.4 and 4.0 is available as Supporting Information.

Modification of PEG-*b*-PLL with DTBP. PEG-*b*-PLL was modified with DTBP under aqueous conditions. Nucleophilic reaction of lysine primary amine groups with imidoester groups contained in DTBP resulted in formation of the amidine with concurrent release of methanol. The reaction pH of 9.0 was chosen to minimize side reactions that are described to occur with imidoesters below pH 8.0.[22] A molar excess amount of DTBP was used to minimize polymer cross-linking, which is expected to occur due to the bifunctional nature of this reagent. A total of 2 molar equiv of DTBP relative to lysine amines used in the polymer modification reaction corresponded to 4 equiv of reactive amido esters. Unreacted DTBP was removed from the reaction mixture prior to disulfide cleavage of polymer-reacted DTBP to allow more efficient reduction with DTT. Reaction of the DTBP-modified polymer with DTT resulted in cleavage of the internal disulfide and generation of the desired 1-(3-mercaptopropyl) amidine functionality. DTT was removed quickly and efficiently (~4 h) using high surface area slide-a-lyzer dialysis cassettes, as DTT was not detected in the ^{1}H NMR spectrum of the obtained product (Figure 2). Successful modification of lysine amines with DTBP was confirmed by ^{1}H NMR spectroscopy, as indicated by the downfield shift of lysine ε-CH_2 groups and the appearance of two methylene peaks corresponding to those found in DTBP (Figure 2). The degree of lysine modification was 95% under the reaction conditions used in this study.

Analysis of Thiol Content in Modified PEG-*b*-PLLs. Free thiol content in PEG-*b*-PLL(N2IM-IM) and PEG-*b*-PLL(MPA) was determined using Ellman's assay, which is based on reaction of 5,5-dithio-bis-(2-nitrobenzoic acid) with sulfhydryls at basic pH to generate a colored thiolate derivative. The measured thiol content was quite different between PEG-*b*-PLL(N2IM-IM) and PEG-*b*-PLL(MPA), as shown in Table 1. PEG-*b*-PLL(MPA) thiol content was near the theoretical value assuming complete reaction of lysine amines (90 ± 10%), whereas PEG-*b*-PLL-(N2IM-IM) thiol content was much lower (11 ± 2%). The low amount of free sulfhydryl detected in PEG-*b*-PLL(N2IM-IM) is consistent with the formation of N-substituted 2-iminothiolanes, which lack free thiol functionality.

Preparation and Characterization of PIC Micelles Formed with siRNA. PIC micelles formed spontaneously upon mixing polymer and siRNA solutions under reducing conditions, as evidenced by increased scattered light intensity and the presence of particles less than 100 nm in size with low PDI (<0.1, i.e., spherical). At pH 7.4, PIC micelles formed at higher polymer/siRNA molar ratios for PEG-*b*-PLL(N2IM-IM) (polymer/siRNA = 3.6−7.6) and only at near stoichiometric ratios for PEG-*b*-PLL(MPA) (polymer/siRNA = 1.0−1.3, Figure 3A). Addition of excess polymer in the case of PEG-*b*-PLL(MPA) resulted in a sharp decrease in SLI, showing that excess polycation disrupts micelle formation. DLS analysis of micelle solutions revealed the formation of narrowly dispersed (PDI <0.1) particles 40−45 nm in size at the optimal polymer/siRNA mixing ratio for both block copolymers, which is consistent with values expected for spherical micelle structures (Table 1). Detailed light scattering data for complexation solutions (non-cross-linked) at each polymer/siRNA molar ratio is available as Supporting Information. Analysis of the ζ-potential of cross-linked micelle structures formed at the optimal polymer/siRNA molar ratio indicated a near-neutral value for both PEG-*b*-PLL(N2IM-IM) and PEG-*b*-PLL(MPA), which is expected for core−shell micelle structures where the core charge is shielded by the PEG corona (Table 1). Essentially no free-thiol was detected in cross-linked micelles prepared with PEG-*b*-PLL(MPA), but ~50% free thiol (relative to the original 11% thiol-containing PLL side chains measured in polymer only) was observed in micelles prepared with PEG-*b*-PLL(N2IM-IM) when subjected to Ellman's assay (Table 1). This result shows that both free thiol content and disulfide cross-linking efficiency was reduced in PEG-*b*-PLL(N2IM-IM).

Complexation behavior between PEG-*b*-PLL(N2IM-IM) and siRNA changed under acidic conditions, whereas PEG-*b*-PLL-(MPA) complexation behavior with siRNA did not (Figure 3B). For PEG-*b*-PLL(N2IM-IM), the polymer/siRNA molar ratios corresponding to the maximum SLI value shifted from ~7.6 to lower values near the stoichiometric region. This observation confirmed that protonation of imines present in N-substituted 2-iminothiolane structures can restore the cationic nature of PEG-*b*-PLL(N2IM-IM). On the other hand, PEG-*b*-PLL(MPA) micelle formation behavior was unaffected by lowering the pH of complexation conditions and the polymer/siRNA molar ratio for maximum SLI remained in the stoichiometric region at both pH 7.4 and 5.0. Micelle size and PDI at the polymer/siRNA molar ratio corresponding to maximum SLI did not change for either polymer upon complexation at lower pH (data not shown).

Fluorescence Quenching Studies. PEG-*b*-PLL(N2IM-IM) and PEG-*b*-PLL(MPA) complexation with siRNA was also investigated by monitoring the fluorescence quenching of Cy3-labeled siRNA (Figure 3C). Fluorescence quenching is expected to occur only upon formation of micelle structures through dye−dye interactions or interaction with amines contained in the micelle core.[23−25] Cy3 fluorescence was quenched considerably upon formation of micelles between both block copolymers and siRNA. For PEG-*b*-PLL(MPA), maximum fluorescence quenching was concurrent with the polymer/siRNA molar ratio that resulted in the maximum SLI observed in light scattering

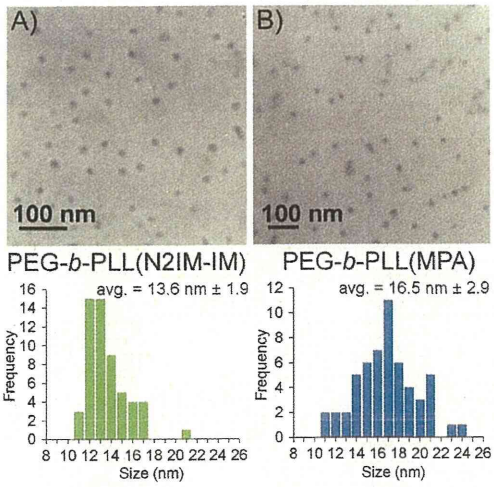

Figure 4. TEM images showing the morphology of cross-linked micelles. (A) PEG-*b*-PLL(N2IM-IM)/siRNA micelles, 80K magnification. (B) PEG-*b*-PLL(MPA) micelles, 50K magnification. The resulting size histograms from measuring the uranyl acetate stained micelle cores are shown below each image.

measurements. Addition of excess PEG-*b*-PLL(MPA) to the complexation mixture resulted in complete recovery of fluorescence intensity, indicating that the micelle structure was not maintained at high polymer/siRNA ratios. However, complexation of Cy3 siRNA with PEG-*b*-PLL(N2IM-IM) resulted in fluorescence quenching at polymer/siRNA ratio of ~1.8 and quenching was maintained up to the polymer/siRNA ratio of 7.6, indicating that polymer/siRNA complexes were unaffected by excess block copolymer. This result corroborates well with light scattering observations where the SLI of solutions prepared with PEG-*b*-PLL(MPA) and siRNA decreased at polymer:siRNA molar ratios greater than ~1.4 (showing micelle dissociation), whereas complexation solutions prepared with PEG-*b*-PLL(N2IM-IM) never exhibited a decrease in SLI up to the polymer/siRNA molar ratio of 7.6 (showing micelle structure is maintained).

In Vitro Micelle Stability. Cross-linked micelle stability was determined as a function of NaCl concentration in the presence or absence of the disulfide reducing agent DTT (Figure 3D). Increased NaCl concentration is expected to interfere with the ionic interactions between cationic polymer and siRNA, thus, disrupting micelle structures. This experiment was not intended to mimic biological conditions, but as a reference, the biological NaCl concentration is ~150 mM. In general, micelles prepared with siRNA and PEG-*b*-PLL(N2IM-IM) were more stable than those prepared with PEG-*b*-PLL(MPA). In the absence of DTT, micelles prepared with PEG-*b*-PLL(N2IM-IM) remained stable up to 600 mM NaCl, whereas micelles prepared with PEG-*b*-PLL(MPA) showed a significant decrease in SLI at 600 mM NaCl. Addition of DTT to the micelle solution resulted in an ~20% decrease in SLI at 600 mM NaCl for PEG-*b*-PLL(N2IM-IM), while the SLI of PEG-*b*-PLL(MPA) micelle solutions decreased to a greater extent (~30–50%) upon disulfide reduction at both 300 and 600 mM NaCl.

Micelle Morphology. Direct observation of cross-linked micelles by TEM showed uniform spherical structures less than 50 nm in size (Figure 4). The dark spheres in the TEM images

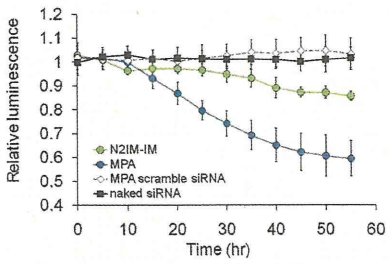

Figure 5. In vitro gene knockdown of luciferase in B16F10-luc cells. SiRNA was incorporated within cross-linked micelles prepared with PEG-*b*-PLL(X) (X = N2IM-IM or MPA) and introduced to cells at 200 nM siRNA. Data is presented as the ratio of treated sample luminescence to nontreated controls ± the standard deviation, $n = 4$.

correspond to the micelle core, as uranyl acetate specifically stains nucleic acids. Micelle core diameters were found to be 13.6 nm for PEG-*b*-PLL(N2IM-IM)/siRNA and 16.5 nm for PEG-*b*-PLL(MPA)/siRNA, both with narrow size distribution.

In Vitro Gene Silencing. The ability of micelles to deliver and release antiluciferase siRNA aimed to inhibit luciferase expression was determined in B16F10 murine melanoma cells stably expressing luciferase. In vitro gene silencing was highest when siRNA was administered encapsulated within micelles prepared with PEG-*b*-PLL(MPA), as shown in Figure 5. PEG-*b*-PLL(MPA)/siRNA micelle treated cells showed a modest (~40%) decrease in luminescence between 10 and 55 h, while PEG-*b*-PLL(N2IM-IM)/siRNA micelles showed a smaller (~12%) decrease in luminescence between 25 and 55 h. No cytotoxicity was observed for PEG-*b*-PLL(N2IM-IM)/siRNA or PEG-*b*-PLL(MPA)/siRNA micelles at siRNA concentrations up to 1000 nM, showing that luciferace knockdown was not due to reduced cell metabolism as a result of micelle introduction (see Supporting Information). Negligible luciferase knockdown was observed for naked siRNA or PEG-*b*-PLL(MPA)/siRNA micelles containing scramble siRNA, indicating that encapsulation within a micelle carrier is essential and also that the gene silencing was due to the siRNA effect and not due to the polymer used for micelle formation. No gene silencing was observed for PEG-*b*-PLL/siRNA micelles prepared at polymer/siRNA molar ratio of 1.2 (Table 1).

In Vivo Micelle Stability. Micelle behavior in the bloodstream was observed in mouse ear lobe dermis following I.V. injection. Naked siRNA was rapidly removed from the bloodstream (Figure 6A), with a half-life of approximately 3 min. Blood circulation time was improved by incorporating siRNA into disulfide-cross-linked micelle carriers, as the half-life increased to ~6 min for micelles prepared with PEG-*b*-PLL(MPA) and ~10 min for micelles prepared with PEG-*b*-PLL(N2IM-IM). Cy5 fluorescence intensity remained high for the first ~2 min for both disulfide-cross-linked micelle formulations but then rapidly decreased for PEG-*b*-PLL(MPA), with a profile similar to naked siRNA. The difference in blood vessel retention is clearly seen in Figure 6C, where Cy5 fluorescence remained high for PEG-*b*-PLL(N2IM-IM)/siRNA micelles after 10 min. No aggregates were visible in the bloodstream for any of the formulations following injection.

Extravasation of Cy5 into the surrounding skin tissue was apparent for naked siRNA and PEG-*b*-PLL(MPA)/siRNA micelles (Figure 6B). Extravasation is expected to occur only for low molecular weight species and, thus, indicates dissociation of the

micelles and possibly degradation of siRNA. Cy5 fluorescence increased in the tissue region more rapidly for PEG-*b*-PLL-(MPA)/siRNA micelles compared to PEG-*b*-PLL(N2IM-IM)/siRNA micelles. Tissue fluorescence for PEG-*b*-PLL(N2IM-IM)/siRNA micelles slowly increased over the 60 min observation period and never peaked (Figure 6B).

DISCUSSION

The focus of this work was to better understand the mechanism of polyion complex micelle formation between PEG-*b*-PLL(N2IM-IM) and siRNA, and also to observe the effects of polymer structure on micelle properties. Interest regarding the mechanism of micelle formation between PEG-*b*-PLL(N2IM-IM) and siRNA was sparked by observations from our previous work which showed that the optimal molar ratio of polymer/siRNA for micelle formation increased with increased IM content in the block copolymer. Further consultation with the literature suggested that the observed complexation behavior could be due to the tendency of 1-(4-mercaptobutyl) amidine groups initially formed following reaction of primary amines with 2-IT to cyclize and form N-substituted 2-iminothiolane moieties. The mechanism proposed for N-substituted 2-iminothiolane formation is shown in Figure 7, reproduced from the work of Mokotoff et al. and Singh et al.[16,17] These authors showed that reaction of primary amines with 2-IT resulted in the formation of linear 1-(4-mercaptobutyl) amidine functional groups initially but this species quickly disappeared along with concurrent appearance of cyclic N-substituted 2-iminothiolane structures. This behavior was also observed following the reaction of glucosamine with 2-IT, and the N-substituted 2-iminothiolane structure was confirmed by mass spectrometry.[26] Formation of the N-substituted 2-iminothiolane rings is rapid at room temperature and slightly basic pH, with half-lives of the initially formed 1-(4-mercaptobutyl) amidine ~0.5−3 h, depending on the pK_a of the amine nucleophile used for reaction with 2-IT. Specifically, the half-life of 1-(4-mercaptobutyl) amidines formed by reaction of 2-IT with amines having a pK_a of 9.3−9.8 (which is similar to the pK_a of lysine amines (~10) used for reaction with 2-IT in this study) is 1.8−2.8 h at pH 8, 25 °C.

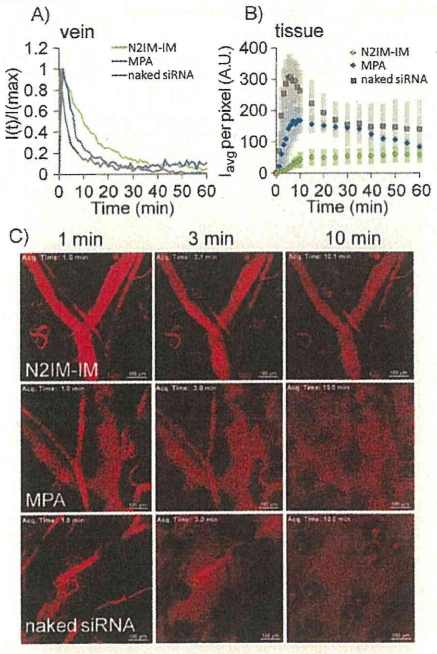

Figure 6. Behavior of siRNA incorporating micelles prepared with PEG-*b*-PLL(X) (X = N2IM-IM or MPA) following intravenous injection. (A) Residence time of Cy5 in the bloodstream normalized to the maximum observed intensity. (B) Cy5 fluorescence in the extravascular skin tissue, each data point represents the mean value ± the standard deviation of four regions of interest. (C) Snapshots of ear lobe dermis at 1, 3, and 10 min with Cy5 fluorescence shown as red. The scale bar represents 100 μm in each image. Representative data from one mouse for each sample is shown in A−C.

Formation of the N-substituted 2-iminothiolane derivative in PEG-*b*-PLL(N2IM-IM) results in a five-membered ring structure. Thus, an appropriate amidination reagent must produce a mercaptoalkyl amidine not capable of ring formation. The chemistry contained in DTBP results in a formation of a 1-(3-mercaptopropyl) amidine group that contains only two carbons between the amidine and thiol and will not recyclize due to the instability of a four-membered ring. Modification of PEG-*b*-PLL with DTBP provided a convenient and stable structure for comparison with PEG-*b*-PLL(N2IM-IM).

^{1}H NMR analysis of PEG-*b*-PLL(N2IM-IM) confirmed that nearly all lysine amines reacted with 2-IT and also provided direct evidence that both cyclic N-substituted 2-iminothiolane and linear 1-(4-mercaptobutyl) amidine groups were present in the product (Figure 2). Generation of the N-substituted 2-iminothiolane has been reported to produce a small upfield shift (~0.2 ppm) of protons adjacent to the imine nitrogen in the ^{1}H NMR spectra of small molecules, and this small shift was also observed in the ^{1}H NMR spectrum of PEG-*b*-PLL(N2IM-IM).[16] The main peak at 3.25 ppm corresponds to lysine ε-CH_2 protons adjacent to N-substituted 2-iminothiolane containing side chains and the shoulder at 3.4 ppm corresponds to lysine ε-CH_2 protons adjacent to 1-(4-mercaptobutyl) amidine containing side chains. Estimation of the ratio of the two side chain structures from

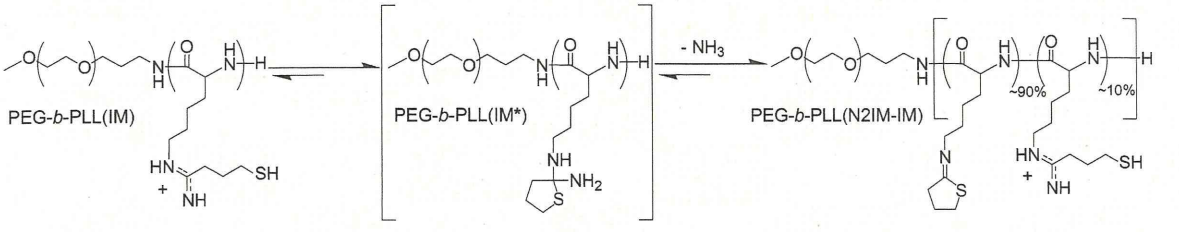

Figure 7. Intramolecular rearrangement of 1-(4-mercaptobutyl) amidine groups in PEG-*b*-PLL(IM) into N-substituted 2-iminothiolane moieties in PEG-*b*-PLL(N2IM-IM) via a tetrahedral intermediate structure. Adopted from Singh et al. and Mokotoff et al. (refs 16 and 17). Residual unmodified lysines are not shown in the chemical structures.

integration values showed that the N-substituted 2-iminothiolane ring is the predominant product following reaction with 2-IT (~75%). It should be noted that reaction of PEG-*b*-PLL with 1 molar equiv of 2-IT resulted in only ~60% conversion of lysine amines despite long (18 h) reaction time (data not shown). Reaction with at least a 2-fold excess of 2-IT is essential to achieve ~100% modification of lysine primary amines under the conditions described here. This is likely due to ammonia generated upon formation of N-substituted 2-iminothiolane rings competing for reaction with 2-IT and thus decreasing lysine amine conversion.

In our previous report, we obtained a product that did not show any N-substituted 2-iminothiolane functionality in the ^{1}H NMR spectrum of isolated polymer product, even at high lysine conversion (see Supporting Information). However, the siRNA complexation behavior at pH 7.4 was nearly identical between the PEG-*b*-PLL(IM) obtained in our previous report and the PEG-*b*-PLL(N2IM-IM) obtained in the current study. We found that treatment of PEG-*b*-PLL(IM) from the previous study with DTT at pH 7.4, and subsequent purification by dialysis, resulted in formation of the N-substituted 2-iminothiolane structures observed in this work (see Supporting Information). Thus, even if N-substituted 2-iminothiolane structures are not observed in the ^{1}H NMR spectrum of product obtained following reaction of PEG-*b*-PLL with 2-IT (at amounts targeting complete conversion of lysines), the ring structures will form upon reduction with DTT in aqueous buffer at pH 7.4. This seems reasonable if the isolated product contains a high degree of disulfide cross-linking, which would prevent the formation of N-substituted 2-iminothiolane rings. Disulfide formation during the reaction of PEG-*b*-PLL with 2-IT is likely why a residual amount of 1-(4-mercaptobutyl) amidine functionality is observed in the polymer product obtained in this study. It should be noted, however, that the structure of functional groups contained in PEG-*b*-PLL lysine side chains following reaction with lower molar ratios of 2-IT may be more complicated. Residual unmodified lysine amines can react with the N2IM structure to generate N,N′-disubstituted amidines, resulting in cross-linked (inter- or intramolecular) lysine side chains.[27] Thus, for simplicity, we targeted complete conversion of lysine amines with 2-IT in this study.

Formation of the N-substituted 2-iminothiolane derivative in PEG-*b*-PLL(N2IM-IM) product was also evidenced by analysis of free thiol content using Ellman's assay, as this cyclic moiety lacks sulfhydryl groups. Free thiol content was much lower for PEG-*b*-PLL(N2IM-IM) compared to PEG-*b*-PLL(MPA), confirming that the majority of modified lysines contained closed ring structures (Table 1). However, a finite amount (~10% of original lysine side chains) of free thiol was detected in PEG-*b*-PLL(N2IM-IM). This residual thiol content allows for the desired ability to form disulfide cross-links in the core of micelles prepared with PEG-*b*-PLL(N2IM-IM) and siRNA.

Polymeric micelles formed spontaneously upon mixing polymer and siRNA solutions in HEPES buffer (pH 7.4) at room temperature (22 °C). Complexation of block copolymer with siRNA was expressed as a function of the molar ratio of polymer/siRNA. We chose this format because of the complexity of the PEG-*b*-PLL(N2IM-IM) side chain structure, which makes exact definition of charge ratio difficult. Another method commonly used to express the polycation/nucleic acid ratio is N/P ratio. In this case, N typically represents the molar equivalent of amines (+ charge) and P represents the molar equivalents of siRNA phosphates (− charge). For polycations used in this study, the polymer/siRNA molar ratio is nearly interchangeable with N/P ratio if the charge is retained (i.e., PEG-*b*-PLL(MPA)), as the GL3 siRNA carries a net charge of (−) 40 and the PLL segment in the polycation block of PEG-*b*-PLL contains 46 units. This degree of polymerization for PLL was targeted so that one polymer chain neutralizes the charge of one siRNA molecule.

In general, modification of PEG-*b*-PLL with either 2-IT or DTBP improved the quality (controlled size and PDI) of micelles formed with siRNA. PEG-*b*-PLL alone formed large particles (~200 nm, PDI = 0.4) with siRNA near stoichiometric molar ratios (Table 1.). Micelle formation behavior between PEG-*b*-PLL(N2IM-IM) or PEG-*b*-PLL(MPA) and siRNA at pH 7.4 was markedly different. PEG-*b*-PLL(N2IM-IM) formed micelles over a broader range of polymer/siRNA molar ratios (~2−7.6) while micelles formed with PEG-*b*-PLL(MPA) only near stoichiometric molar ratios, with light scattering and fluorescence quenching results in good agreement (Figure 3A and 3C). Micelles formed at the polymer/siRNA molar ratio corresponding to the highest SLI value for both polymers were narrowly dispersed spherical structures as evidenced by the low PDI value obtained in DLS measurement (Table 1) and also by direct TEM observation (Figure 4). Excess polycation inhibited micelle formation in the case of PEG-*b*-PLL(MPA), as the SLI decreased and Cy3-siRNA fluorescence recovered at polymer/siRNA molar ratios above ~1.4 (Figure 3A,C). PEG-*b*-PLL-(MPA) retains positive charge due to basic amidine groups (pK_a~11−12) and rearrangement of side chains into N-substituted 2-iminothiolane structures with a lower pK_a is prevented due to the shorter methylene spacer between the amidine and thiol.[28] The fact that micelles remain present in complexation mixtures containing a molar excess of PEG-*b*-PLL(N2IM-IM) suggests that this polymer is less charged than PEG-*b*-PLL-(MPA), which is expected due to the prevalence of imines with a lower pK_a. Residual 1-(4-mercaptobutyl) amidine groups (which contain amidine functionality and thus positive charge) as well as unreacted lysine amines in PEG-*b*-PLL(N2IM-IM) likely provide the driving force for polymer association with siRNA through long-range Coulombic interactions. After polymer chains assemble in close proximity, additional short-range nonionic interactions (van der Waals, dipole−dipole, H-bonding) may occur to further stabilize the structure. When the residual charge of PEG-*b*-PLL(N2IM-IM) is considered (~5% unreacted lysines determined by ^{1}H NMR and 11% residual 1-(4-mercaptobutyl) amidines determined by Ellman's assay), a ± charge ratio of ~1.4 is calculated at the polymer/siRNA molar ratio of 7.6, where maximum SLI is observed. Assuming that all modified PLL side chains are charged in PEG-*b*-PLL(MPA), the polymer/siRNA molar ratio that resulted in maximum SLI corresponds to a ± ratio of 1.3. Thus, the ± charge ratio corresponding to maximum SLI were nearly the same for both PEG-*b*-PLL(N2IM-IM) and PEG-*b*-PLL(MPA) polymers at pH 7.4.

The effect of N-substituted 2-iminothiolane ring structures on block copolymer complexation with siRNA was confirmed by lowering the pH of complexation solutions. Formation of N-substituted 2-iminothiolane groups results in the loss of highly basic amidine groups and concurrent formation of imines of lower pK_a. For example, the pK_a value reported for an imine group contained in a N-substituted 2-iminothiolane formed by reaction of 2-IT with ethanolamine is reported as 6.7, which would result in a drastic loss of charge at pH 7.4 compared to the parent amidine.[16] At acidic complexation conditions

PEG-*b*-PLL(N2IM-IM) and PEG-*b*-PLL(MPA) behaved similarly, with micelles forming only at polymer/siRNA molar ratios near the stoichiometric region (Figure 3B). At pH 5.0, the imine groups of PEG-*b*-PLL(N2IM-IM) were protonated and, thus, cationic nature was restored, which in turn aligned the complexation behavior to that observed with PEG-*b*-PLL(MPA). Interestingly, although protonation of imines altered micelle formation behavior between PEG-*b*-PLL(N2IM-IM) and siRNA, incubation of cross-linked micelles (following disulfide reduction at pH 7.4) at pH 4.0 did not disrupt the micelle structure even at 150 mM NaCl (see Supporting Information). This treatment resulted in micelle swelling, but not micelle disruption.

Results with PEG-*b*-PLL(MPA) as well as protonated PEG-*b*-PLL(N2IM-IM) suggest that excess polycation disrupts micelle formation between block copolymers and siRNA. In the case of PEG-*b*-PLL(N2IM-IM), reduced polymer charge upon formation of N-substituted 2-iminothiolane rings likely reduced electrostatic repulsion between polymer chains and also competition for siRNAs, allowing more polymer to associate with micelle structures. Additionally, PEG-*b*-PLL(N2IM-IM) exhibited maximum fluorescence quenching at a lower polymer/siRNA molar ratio than that corresponding to the maximum SLI value (~7.6) and quenching was maintained over the entire range of polymer concentrations tested. This suggests that the polymer significantly interacts with siRNA at polymer/siRNA molar ratios ≥ 1.8, as evidenced by the change in the Cy3 microenvironment leading to quenching. However, polymer association is not complete until polymer:siRNA molar ratios of ~7.6, where maximum SLI was observed. This is consistent with our previous gel retardation studies of micelles prepared with siRNA and PEG-*b*-PLL(N2IM-IM), where siRNA did not enter the gel for complexation solutions prepared at polymer/siRNA ratios >2.7.[14]

Micelle *z*-average diameters measured by DLS and micelle core sizes determined by TEM were in good agreement, and the sizes obtained were similar for both PEG-*b*-PLL(N2IM-IM) and PEG-*b*-PLL(MPA) (Table 1 and Figure 4). Low PDI values obtained by DLS measurement of polymer/siRNA assemblies suggests that spherical structures formed, which was confirmed by direct TEM observation of cross-linked micelles. As expected, micelle diameters determined by DLS analysis were larger than the core size of micelles determined from the TEM images. However, the determined size of micelle cores by TEM corroborated well with whole micelle size values observed by DLS, considering the size of PEG and assuming a core−shell micelle structure. The radius of gyration (R_g) of PEG 12K in water is 4.68 nm; thus, the tethered PEG chain height is 9.36 nm ($2 \times R_g$) in the so-called mushroom or random coil conformation.[29,30] Addition of the PEG segment length to the measured micelle core size obtained from TEM images results in a calculated diameter of 32.3 nm for PEG-*b*-PLL(N2IM-IM)/siRNA micelles and 35.2 nm for PEG-*b*-PLL(MPA)/siRNA micelles, which are less than the *z*-average values reported in Table 1. Conversion of DLS data to number average diameters directly from the size distribution histogram generated from the ZetaSizer software resulted in a calculated diameter of 32.0 ± 2.37 nm for PEG-*b*-PLL(N2IM-IM)/siRNA micelles and 32.4 nm ±1.3 nm for PEG-*b*-PLL(MPA)/siRNA micelles, which is in excellent agreement with calculated diameters from TEM images (see Supporting Information). Micelle core diameters measured from TEM imaging were smaller for PEG-*b*-PLL(N2IM-IM)/siRNA, while the whole micelle diameter measured by DLS was the same for both PEG-*b*-PLL(N2IM-IM) and PEG-*b*-PLL(MPA). This suggests that the PEG layer may be thicker in PEG-*b*-PLL(N2IM-IM)/siRNA micelles, where PEG chains become more elongated on the micelle surface due to the close proximity of other chains. This seems reasonable as more polymer may be associating with PEG-*b*-PLL(N2IM-IM)/siRNA micelles, which form in the presence of ~7.6 times molar excess of polymer. Altogether, micelle characterization by both DLS and TEM further support that core−shell micelle structures are formed upon association of polymer with siRNA at the polymer:siRNA molar ratio corresponding to maximum SLI.

Modification of PEG-*b*-PLL with 2-IT or DTBP increased the stability of PIC micelles formed with siRNA as evidenced by the maintenance of micelle structures formed with both block copolymers up to 300 mM NaCl (Figure 3D), whereas non-cross-linked assemblies (but not necessarily individual polyion complexes) formed between siRNA and PEG-*b*-PLL nearly completely dissociate in 150 mM NaCl.[14] However, PEG-*b*-PLL(N2IM-IM)/siRNA micelles were ultimately more stable than PEG-*b*-PLL(MPA)/siRNA micelles at high NaCl concentration (600 mM). This suggests that nonionic interactions, such as van der Waals, ion-dipole, or H-bonding (via imine nitrogens) may also contribute to micelle stability. Incubation of PEG-*b*-PLL(N2IM-IM)/siRNA micelles in a high ionic strength solution under reductive conditions resulted in disruption of micelle structures (~20% decrease in SLI compared to nonreductive conditions), showing that disulfide cross-links did in fact contribute to micelle stability.

For PEG-*b*-PLL(MPA), dissociation of micelles at high NaCl concentration in the absence of DTT suggests that disulfide cross-linking alone did not provide the same stability provided by PEG-*b*-PLL(N2IM-IM), which had a much lower thiol content and disulfide formation efficiency in the micelle core. However, the degree of intermolecular vs intramolecular disulfide cross-linking in PEG-*b*-PLL(MPA)/siRNA micelles is unknown, and only the former would result in increased micelle stability in the absence of disulfide reducing agents. Micelles formed with PEG-*b*-PLL(MPA) were more sensitive to dissociation in the presence of DTT, indicating that disulfide cross-linking was more critical to improving the stability of micelles prepared solely from electrostatic interactions.

In vitro gene silencing activity of siRNA was improved upon encapsulation within polymeric micelle carriers prepared from PEG-*b*-PLL(N2IM-IM) or PEG-*b*-PLL(MPA), as no gene silencing was observed for naked siRNA or PEG-*b*-PLL particles (Figure 5 and Table 1). Gene silencing was highest for PEG-*b*-PLL(MPA)/siRNA micelles, which may be attributed to higher sensitivity to disulfide reduction. PEG-*b*-PLL(MPA)/siRNA micelles likely dissociate more readily once internalized into cells, thus, releasing the siRNA cargo. This is consistent with the observed difference in lag time before gene silencing, where PEG-*b*-PLL(MPA)/siRNA micelles showed gene silencing after only 10 h and PEG-*b*-PLL(N2IM-IM)/siRNA micelles showed gene silencing after 25 h. More stable PEG-*b*-PLL(N2IM-IM) micelles likely dissociate and release siRNA more slowly, thus, requiring more time before gene knockdown is observed. Nonetheless, the fact that gene silencing was observed after 55 h of incubation indicates that both micelle structures were effective at protecting siRNA from degradation into inactive fragments within the cell culture medium or off-target sites within the subcellular environment.

One of our goals regarding development of a siRNA delivery system is to produce a carrier that has prolonged residence time

in the bloodstream, allowing the carrier to be administered by I.V. injection. Polymer/siRNA micelle structures obtained in this study are particularly attractive candidates for cancer treatment by I.V. injection as they are large enough to escape rapid renal filtration (~ 10 nm cutoff) but small enough (<100 nm) to gain tumor mass accumulation by the enhanced permeability and retention (EPR) effect.[31,32] Thus, we investigated the blood circulation time of micelles prepared in this work. In order to have prolonged blood circulation the carrier must not interact with blood components (leading to aggregation or micelle dissociation) and must also remain intact to protect siRNA from premature release and degradation. Blood circulation results clearly identify that micelles prepared with PEG-*b*-PLL(N2IM-IM) and siRNA remain in the bloodstream longer than any other formulation tested (Figure 6A). Micelles prepared with PEG-*b*-PLL(MPA) provided some improvement in blood residence time compared to naked siRNA and PEG-*b*-PLL/siRNA particles. This result suggests that even a high degree of disulfide cross-linking was insufficient to greatly prolong residence time in the bloodstream. However, although disulfide formation efficiency was high for PEG-*b*-PLL(MPA)/siRNA micelles, the amount of intermolecular cross-linking is unknown. A longer spacer between the amidine and thiol in modified PLL side-chains may further improve micelle stability and blood residence time.

Improved blood circulation for PEG-*b*-PLL(N2IM-IM)/siRNA micelles may not be solely linked to micelle stability. As mentioned previously, the PEG density is likely higher for micelles formed with PEG-*b*-PLL(N2IM-IM) than those prepared with PEG-*b*-PLL(MPA) as the former were prepared at a higher molar ratio of polymer. Higher PEG density may further reduce nonspecific interactions of micelles with blood components leading to longer circulation time. The impact of PEG density on stability in the blood compartment is beyond the scope of this study but we hope to clarify this in the future. Furthermore, the lower charge density of PEG-*b*-PLL(N2IM-IM) likely results in diffuse charges in the micelle core which in turn could reduce interactions with charged (mainly anionic) components in the bloodstream.

In addition to providing the longest blood circulation time, micelles prepared with PEG-*b*-PLL(N2IM-IM) also showed the lowest increase in tissue fluorescence outside of blood vessels. Extravasation into surrounding tissues suggests that micelle structures dissociated and fluorescent labeled siRNA was released and possibly degraded, producing small fragments of siRNA with high tissue permeability. We have previously observed such effects with fluorescein and fluorescein-labeled dextrans. In that study, we observed that free dye and dye-labeled dextrans lower than ~10 kDa quickly entered the tissue following I.V. injection, whereas higher MW dye-labeled dextrans did not.[21] Thus reduced migration of Cy5 fluorescence into the tissue region surrounding blood vessels in the case of PEG-*b*-PLL(N2IM-IM)/siRNA micelles provides further evidence that micelles remained intact in the bloodstream.

In summary, we found that a highly charged cationic block copolymer was not necessary to form micellar structures with siRNA. PEG-*b*-PLL(N2IM-IM) formed micelles with siRNA despite loss of a large percentage of charged amidine groups. This block copolymer likely retained enough residual charge to interact with siRNA and assemble into higher-ordered micellar structures but not so much charge as to electrostatically repel itself at high polymer concentrations. The unique association behavior of PEG-*b*-PLL(N2IM-IM) and siRNA represents a nontraditional PIC assembly where the polycation contains low charge density and micelles form in the presence of excess block copolymer. In this regard, PEG-*b*-PLL(N2IM-IM)/siRNA micelles are attractive from a practical point of view because micelle formation is less sensitive to slight variations in polymer concentration. In contrast, strongly charged PEG-*b*-PLL(MPA) cationic block copolymer showed very sensitive micelle formation behavior with siRNA and excess polycation inhibited micelle assembly. Inhibition of micelle formation was likely due to repulsion of charged polymer chains and increased competition with siRNAs. As a result, preparation of micelles with PEG-*b*-PLL(MPA) and siRNA required careful control of polymer and siRNA mixing ratios.

Covalent disulfide cross-linking is expected to improve micelle stability compared to particles prepared from unmodified PEG-*b*-PLL, but a high thiol-content block copolymer did not produce the most stable micelle structure in this work. Micelles prepared from polymer comprising relatively low free thiol content were more resistant to dissociation in vitro and also exhibited longer residence time in the bloodstream in vivo. The possibility of noncovalent interactions between polymer chains in addition to covalent disulfide cross-linking greatly improved micelle stability. Improved micelle stability came at a performance cost, as noncovalent polymer interactions in addition to covalent disulfide cross-links reduced the sensitivity of micelles to disruption under disulfide reducing conditions. Increased stability and reduced sensitivity to disulfide reduction were likely responsible for the increased lag-time observed for the onset of gene silencing in cell culture experiments. On the other hand, the benefit of preparing stable micelles with high polymer content was realized in vivo. Micelles prepared with PEG-*b*-PLL(N2IM-IM) exhibited longer blood circulation, which is necessary for I.V. administration of siRNA delivery systems. Thus, the chemistry contained in the block copolymer must be carefully controlled to produce effective siRNA carriers on the cellular and whole organism level.

Understanding the mechanisms that govern the assembly and stability of nanoparticles is crucial for improvements of their design. The findings of this work may be further generalized in the sense that "soft" polycations containing less positive charge and "hard" polycations with high charge density differ in their complexation behavior with siRNA. While interactions between polyelectrolytes can provide the driving force for particle assembly, the stability of the resulting polyplex may be further enhanced by contributions from nonionic interactions in addition to covalent cross-links to form more robust structures. Formation of micelle structures between polymers and siRNA may be more sensitive to the chemistries contained in the polymer component than large polyanions such as plasmid DNA (pDNA). siRNA is much smaller than pDNA and cannot condense and adopt different conformations in response to excess polycation. Instead, siRNA can simply dissociate from the polyion complex due to the increased mobility of a shorter polyanion. Preparation of stable siRNA polymeric micelle nanocarriers is hinged on a delicate balance of chemistries contained in the polymer component.

CONCLUSIONS

In this work, we found that a high degree of PEG-*b*-PLL modification with 2-iminothiolane resulted in the formation of N-substituted 2-iminothiolane structures in the majority of reacted lysine side chains. This chemistry reduced the polymer charge density at pH 7.4, which in turn shifted the optimal conditions of micelle formation to favor higher molar ratios of

polymer/siRNA compared to a highly charged block copolymer. Despite lower free thiol content and disulfide cross-linking efficiency, micelles formed with PEG-*b*-PLL(N2IM-IM) and siRNA were more stable in buffer and in the bloodstream compared to those formed with PEG-*b*-PLL(MPA) and siRNA. These results highlight the importance of nonionic and noncovalent interactions toward the stability of micelles formed between siRNA and block copolymers. However, higher micelle stability and loss of sensitivity to disulfide reducing conditions resulted in lower siRNA activity on the cellular level; thus, reversible micelle stability is critical to achieve high gene silencing at the target site. The siRNA encapsulating micelles described in this work are promising candidates as carriers for siRNA delivery applications and our efforts to correlate micelle properties with in vitro and in vivo efficacy are ongoing.

■ ASSOCIATED CONTENT

Supporting Information. Figures showing (1) a summary of scattered light intensity, size, and PDI of micelles (non-cross-linked) contained in PEG-*b*-PLL(N2IM-IM)/siRNA solutions at various polymer concentrations, (2) scattered light intensity, size, and PDI of PEG-*b*-PLL(N2IM-IM) polymer solutions at pH 7.4 and 4.0, (3) scattered light intensity of cross-linked PEG-*b*-PLL(N2IM-IM) micelles at pH 7.4 and pH 4.0 at various micelle concentrations, (4) size distribution histograms of cross-linked micelles determined by DLS, (5) ^{1}H NMR analysis of PEG-*b*-PLL(IM) following reduction in DTT at pH 7.4, (6) cytotoxicity of polymer/siRNA micelles prepared with PEG-*b*-PLL(N2IM-IM) and PEG-*b*-PLL(MPA), and (7) blood circulation profile of cross-linked micelles in different mice ($n = 2$) are provided. This material is available free of charge via the Internet at http://pubs.acs.org.

■ AUTHOR INFORMATION

Corresponding Author

*Tel.: +81-3-5841-7138. Fax: +81-3-5841-7139. E-mail: kataoka@bmw.t.u-tokyo.ac.jp.

■ ACKNOWLEDGMENT

This research was financially supported by the Funding Program for World-Leading Innovative R&D in Science and Technology (FIRST), the Japan Society for the Promotion of Science (JSPS), and the Core Research Program for Evolutional Science and Technology (CREST) from the Japan Science and Technology Agency (JST).

■ REFERENCES

(1) Whitehead, K.; Langer, R.; Anderson, D. *Nat. Rev. Drug Discovery* **2009**, *8*, 129–138.
(2) Gary, D.; Puri, N.; Won, Y. *J. Controlled Release* **2007**, *121*, 64–73.
(3) Juliano, R.; Alam, M.; Dixit, V.; Kang, H. *Nucleic Acids Res.* **2008**, *36*, 4158–4171.
(4) Ai, H.; Jones, S.; Lvov, Y. *Cell Biochem. Biophys.* **2003**, *39*, 23–43.
(5) Hammond, P. *Adv. Mater.* **2004**, *16*, 1271–1293.
(6) Christie, R.; Nishiyama, N.; Kataoka, K. *Endocrinology* **2010**, *151*, 466–473.
(7) Wang, Y.; Angelatos, A.; Caruso, F. *Chem. Mater.* **2008**, *20*, 848–858.
(8) Mintzer, M.; Simanek, E. *Chem. Rev.* **2009**, *109*, 259–302.
(9) Meyer, M.; Philipp, A.; Oskuee, R.; Schmidt, C.; Wagner, E. *J. Am. Chem. Soc.* **2008**, *130*, 3272–3273.
(10) Lee, Y.; Miyata, K.; Oba, M.; Ishii, T.; Fukushima, S.; Han, M.; Koyama, H.; Nishiyama, N.; Kataoka, K. *Angew. Chem., Int. Ed.* **2008**, *47*, 5163–5166.
(11) Convertine, A.; Benoit, D.; Duvall, C.; Hoffman, A.; Stayton, P. *J. Controlled Release* **2009**, *133*, 221–229.
(12) Takae, S.; Miyata, K.; Oba, M.; Ishii, T.; Nishiyama, N.; Itaka, K.; Yamasaki, Y.; Koyama, H.; Kataoka, K. *J. Am. Chem. Soc.* **2008**, *130*, 6001–6009.
(13) Miyata, K.; Kakizawa, Y.; Nishiyama, N.; Harada, A.; Yamasaki, Y.; Koyama, H.; Kataoka, K. *J. Am. Chem. Soc.* **2004**, *126*, 2355–2361.
(14) Matsumoto, S.; Christie, R.; Nishiyama, N.; Miyata, K.; Ishii, A.; Oba, M.; Koyama, H.; Yamasaki, Y.; Kataoka, K. *Biomacromolecules* **2009**, *10*, 119–127.
(15) Meister, A.; Anderson, M. *Annu. Rev. Biochem.* **1983**, *52*, 711–760.
(16) Singh, R.; Kats, L.; Blattler, W.; Lambert, J. *Anal. Biochem.* **1996**, *236*, 114–125.
(17) Mokotoff, M.; Mocarski, Y.; Gentsch, B.; Miller, M.; Zhou, J.; Chen, J.; Ball, E. *J. Pept. Res.* **2001**, *57*, 383–389.
(18) Harada, A.; Kataoka, K. *Macromolecules* **1995**, *28*, 5294–5299.
(19) Ellman, G. *Arch. Biochem. Biophys.* **1959**, *82*, 70–77.
(20) Tam, J. P.; Wu, C. R.; Liu, W.; Zhang, J. W. *J. Am. Chem. Soc.* **1991**, *113*, 6657–6662.
(21) Matsumoto, Y.; Nomoto, T.; Cabral, H.; Matsumoto, Y.; Watanabe, S.; Christie, R. J.; Miyata, K.; Oba, M.; Ogura, T.; Yamasaki, Y.; Nishiyama, N.; Yamasoba, T.; Kataoka, K. *Biom. Opt. Express* **2010**, *1*, 1209–1216.
(22) Browne, D.; Kent, S. *Biochem. Biophys. Res. Commun.* **1975**, *67*, 126–132.
(23) Gruber, H.; Hahn, C.; Kada, G.; Riener, C.; Harms, G.; Ahrer, W.; Dax, T.; Knaus, H. *Bioconjugate Chem.* **2000**, *11*, 696–704.
(24) Berlier, J.; Rothe, A.; Buller, G.; Bradford, J.; Gray, D.; Filanoski, B.; Telford, W.; Yue, S.; Liu, J.; Cheung, C.; Chang, W.; Hirsch, J.; Beechem, J.; Haugland, R. *J. Histochem. Cytochem.* **2003**, *51*, 1699–1712.
(25) Anbazhagan, V.; Kathiravan, A.; Jhonsi, M.; Renganathan, R. *Z. Phys. Chem.* **2007**, *221*, 929–939.
(26) Kafedjiiski, K.; Krauland, A.; Hoffer, M.; Bernkop-Schnurch, A. *Biomaterials* **2005**, *26*, 819–826.
(27) Hahn, F.; Mullen, K.; Schepers, U. *Synlett* **2008**, *18*, 2785–2790.
(28) Koppel, I.; Koppel, J.; Leito, I.; Green, L. *J. Phys. Org. Chem.* **1996**, *9*, 265–268.
(29) Kawaguchi, S.; Imai, G.; Suzuki, J.; Miyahara, A.; Kitano, T. *Polymer* **1997**, *38*, 2885–2891.
(30) Kenausis, G.; Voros, J.; Elbert, D.; Huang, N.; Hofer, R.; Ruiz-Taylor, L.; Textor, M.; Hubbell, J.; Spencer, N. *J. Phys. Chem. B* **2000**, *104*, 3298–3309.
(31) Choi, H.; Liu, W.; Misra, P.; Tanaka, E.; Zimmer, J.; Ipe, B.; Bawendi, M.; Frangioni, J. *Nat. Biotechnol.* **2007**, *25*, 1165–1170.
(32) Maeda, H.; Wu, J.; Sawa, T.; Matsumura, Y.; Hori, K. *J. Controlled Release* **2000**, *65*, 271–284.

Journal of Controlled Release 151 (2011) 104–109

Contents lists available at ScienceDirect

Journal of Controlled Release

journal homepage: www.elsevier.com/locate/jconrel

Concept Paper

In situ quantitative monitoring of polyplexes and polyplex micelles in the blood circulation using intravital real-time confocal laser scanning microscopy

Takahiro Nomoto [a,1], Yu Matsumoto [b,c,d,1], Kanjiro Miyata [b], Makoto Oba [e], Shigeto Fukushima [f], Nobuhiro Nishiyama [b], Tatsuya Yamasoba [c], Kazunori Kataoka [a,b,f,*]

[a] *Department of Bioengineering, Graduate School of Engineering, The University of Tokyo, Japan*
[b] *Division of Clinical Biotechnology, Center for Disease Biology and Integrative Medicine, Graduate School of Medicine, The University of Tokyo, Japan*
[c] *Department of Otorhinolaryngology and Head and Neck Surgery, Graduate School of Medicine and Faculty of Medicine, The University of Tokyo, Japan*
[d] *Department of Otorhinolaryngology and Head and Neck Surgery, Mitsui Memorial Hospital, Japan*
[e] *Department of Vascular Regeneration, Division of Tissue Engineering, The University of Tokyo Hospital, Japan*
[f] *Department of Materials Engineering, Graduate School of Engineering, The University of Tokyo, Japan*

ARTICLE INFO

Article history:
Received 12 January 2011
Accepted 10 February 2011
Available online 3 March 2011

Keywords:
Intravital confocal microscopy
Polyplex
Polyethylene glycol
Block copolymer
Polymer micelle

ABSTRACT

Surface modification using poly(ethylene glycol) (PEG) is a widely used strategy to improve the biocompatibility of cationic polymer-based nonviral gene vectors (polyplexes). A novel method based on intravital real-time confocal laser scanning microscopy (IVRTCLSM) was applied to quantify the dynamic states of polyplexes in the bloodstream, thereby demonstrating the efficacy of PEGylation to prevent their agglomeration. Blood flow in the earlobe blood vessels of experimental animals was monitored in a noninvasive manner to directly observe polyplexes in the circulation. Polyplexes formed distinct aggregates immediately after intravenous injection, followed by interaction with platelets. To quantify aggregate formation and platelet interaction, the coefficient of variation and Pearson's correlation coefficient were adopted. In contrast, polyplex micelles prepared through self-assembly of plasmid DNA with PEG-based block catiomers had dense PEG palisades, revealing no formation of aggregates without visible interaction with platelets during circulation. This is the first report of *in situ* monitoring and quantification of the availability of PEGylation to prevent polyplexes from agglomeration over time in the blood circulation. This shows the high utility of IVRTCLSM in drug and gene delivery research.

1. Concept of new methodologies

Gene therapy offers a unique potential for the treatment of genetic and intractable diseases and for tissue engineering. Its success is dependent upon the development of useful gene vectors as well as application of a drug delivery system (DDS). Nonviral gene vectors are attractive alternatives to viral gene vectors because they are much simpler to produce, transport and store, and induce fewer immune responses. Cationic polymers that electrostatically interact with plasmid DNA (pDNA) have been widely studied as materials to construct nonviral gene vectors [1–5]. The cationic polymers most commonly used as gene vectors include branched polyethylenimine (BPEI), linear polyethylenimine, poly(L-lysine) (PLys), chitosan, and dendrimers [6]. These polymers form polyion complexes (polyplexes) with pDNA to successfully transfer it into cultured cells to induce appreciable level of gene expression. However, these polyplexes have biocompatibility problems for systemic application. Polyplexes usually require excess polycations to generate electrostatic repulsion for their increased solubility and colloidal stability. This eventually results in a shift of their surface charge to a positive value. This positive charge causes nonspecific interaction with anionic components in the body such as plasma proteins and blood cells, which might lead to severe adverse effects [7,8]. Attachment of hydrophilic polymers such as poly(ethylene glycol) (PEG) is called "PEGylation" and has often been used to shield nonviral gene vectors from undesired interaction in the blood. PEGylation also contributes to diminished uptake by the reticuloendothelial system or macrophages, and hence the half-life in blood circulation can be extended.

It is well documented that a PEG palisade prevents nonspecific interaction with biological components. However, *in situ* evaluation of

Abbreviations: PEG, poly(ethylene glycol); DDS, drug delivery system; pDNA, plasmid DNA; BPEI, branched polyethylenimine; PLys, poly(L-lysine); PEG-PLys, poly(ethylene glycol)-*b*-poly(L-lysine); PAsp(DET), poly{*N*-[*N*-(2-aminoethyl)-2-aminoethyl]aspartamide}; PEG-PAsp(DET), poly(ethylene glycol)-*b*-poly{*N*-[*N*-(2-aminoethyl)-2-aminoethyl] aspartamide}; IVRTCLSM, intravital real-time confocal laser scanning microscopy; CV, coefficient of variation; PCC, Pearson's correlation coefficient.

* Corresponding author at: Department of Materials Engineering, Graduate School of Engineering, The University of Tokyo, 7-3-1 Hongo, Bunkyo-ku, Tokyo 113-0033, Japan. Tel.: +81 3 5841 7138; fax: +81 3 5841 7139.
E-mail address: kataoka@bmw.t.u-tokyo.ac.jp (K. Kataoka).
[1] These authors equally contributed to this work.

0168-3659/$ – see front matter © 2011 Elsevier B.V. All rights reserved.
doi:10.1016/j.jconrel.2011.02.011

the interaction between nonviral gene vectors and biological components has not been reported due to the absence of methodology to quantify the interaction. We recently described a method of direct and instantaneous observation of intravenously injected substances using intravital real-time confocal laser scanning microscopy (IVRTCLSM) [9]. IVRTCLSM provides high-speed scanning and simultaneous capture of multicolor fluorescence. The macromolecular agents flowing in the bloodstream in tumors, kidneys, and livers can be monitored using IVRTCLSM.

In the present study, we applied IVRTCLSM for the investigation of the interaction between nonviral gene vectors and biological components *in situ*. For the PEGylated polyplexes, we focused on polyplex micelles made through the self-assembly of pDNA with PEG-based cationic block copolymers [10–12]. We further developed an analytical methodology to quantify the dynamic states of nonviral gene vectors circulating in the bloodstream. This is the first report visualizing and quantifying the interaction between nonviral gene vectors and biological components over time and in real-time *in situ*.

2. Experimental methods

2.1. Sample preparation

Sterile Hepes (1 M, pH 7.3) was purchased from Amresco (Solon, OH, USA) and used as a buffer solution after dilution with distilled water. pDNA encoding the soluble form of vascular endothelial growth factor receptor-1 was labeled with Cy5 using Label IT Tracker Nucleic Acid Localization Kits (Mirus Bio Corporation, Madison, WI, USA). BPEI (molecular weight (MW) 22 kDa; Sigma-Aldrich, St. Louis, MO, USA) was dialyzed in 0.01 M HCl and lyophilized as a hydrochloride salt. BPEI and PLys (hydrobromide salt, MW 4–15 kDa; Sigma-Aldrich) were mixed with Cy5-labeled pDNA (150 μg/mL) at an N/P ratio of 6 and 2, respectively, to form polyplexes. The N/P ratio was defined as the residual molar ratio of amino groups of cationic segment to phosphate groups of pDNA. Poly{*N*-[*N*-(2-aminoethyl)-2-aminoethyl]aspartamide} (PAsp(DET)) (polymerization degree: 95) was synthesized as described previously [13]. PAsp(DET) was mixed with Cy5-labeled pDNA at an N/P ratio of 4. Poly(ethylene glycol)-*b*-poly(L-lysine) (PEG-PLys; MW of PEG: 12,000; polymerization degree of PLys segment: 45) was synthesized as described previously [14]. Poly(ethylene glycol)-*b*-poly{*N*-[*N*-(2-aminoethyl)-2-aminoethyl]aspartamide} (PEG-PAsp(DET); MW of PEG: 12,000 Da; polymerization degree of PAsp(DET) segment: 93) was synthesized by the aminolysis of PEG-poly(β-benzyl L-aspartate) block copolymer with diethylenetriamine according to a previous report [13]. PEG-PLys/pDNA and PEG-PAsp(DET)/pDNA micelles were prepared at an N/P ratio of 2 and 4, respectively. The final Cy5-labeled pDNA concentration was adjusted to 100 μg/mL in 10 mM Hepes buffer (pH 7.3).

2.2. Animal preparation

All animal experimental procedures were executed in accordance with the Guide for the Care and Use of Laboratory Animals as stated by the National Institutes of Health. Balb/c nude mice (female; Charles River Laboratories, Tokyo, Japan) were anesthetized with 3.0%–4.0% isoflurane (Abbott Japan Co., Ltd., Tokyo, Japan) using a Univenter 400 Anaesthesia Unit (Univentor Ltd., Zejtun, Malta). Mice were then subjected to lateral tail vein catheterization with a 30-gauge needle (Dentronics Co., Ltd., Tokyo, Japan) connected to a nontoxic, medical grade polyethylene tube (Natsume Seisakusho Co., Ltd., Tokyo, Japan). Platelets were labeled *in vivo* with the intravenous injection of DyLight 488-conjugated anti-GPIbβ antibody (X488; EMFRET Analytics, Eibelstadt, Germany) following the manufacturer's instructions. Mice were placed onto a custom-designed temperature-controlled microscope stage. The ear lobe was attached beneath the cover slip with a single drop of immersion oil as described in our previous report [9]. Video acquisition of the dermis tissue at a speed of 30 frames per second was performed for 10 min. Two-hundred microliters of naked pDNA, polyplexes, and micelles (20 μg of pDNA) were administered via the tail vein catheter 10 s after video acquisition was initiated. For the platelet inhibition study, 300 μL of aspirin (acetylsalicylic acid; Sigma-Aldrich) saturated aqueous solution was orally administered to mice for 2 consecutive days before IVRTCLSM.

2.3. IVRTCLSM imaging and processing

All picture/movie acquisitions were performed using a Nikon A1R confocal laser scanning microscope system attached to an upright ECLIPSE FN1 machine equipped with a CFI Apo 40× WI λS objective lens (Nikon, Tokyo, Japan). All pictures/movies were acquired at a scale of 79.55 μm × 79.55 μm with 5.11 μm of confocal slice. Acquired data were further processed using Nikon NIS Elements software. The region of interest (ROI) was manually defined in the vein. Image frames were extracted every 5 s from the video data for further analyses. For quantification of aggregates, the coefficient of variation (CV) of Cy5 fluorescence was calculated. For the platelet interaction study, colocalization between DyLight and Cy5 was evaluated by Pearson's correlation coefficient (PCC) [15]. All obtained values were plotted against time.

3. Discovery

3.1. Real-time observation of aggregates

We prepared BPEI/pDNA (N/P = 6), PLys/pDNA (N/P = 2), and PAsp(DET)/pDNA (N/P = 4) polyplexes as well as PEG-PLys/pDNA (N/P = 2) and PEG-PAsp(DET)/pDNA (N/P = 4) micelles. BPEI/pDNA was used as the representative polyplex containing excessive polycations. N/P ratios of PLys/pDNA and PAsp(DET)/pDNA were determined as the critical ratio to condense pDNA according to our previous report [16]. N/P ratios of PEG-PLys/pDNA and PEG-PAsp(DET)/pDNA micelles were determined at the same N/P ratios of PLys/pDNA and PAsp(DET)/pDNA polyplexes, respectively. The size and zeta potentials of these polyplexes and polyplex micelles were summarized in Supplementary Table 1.

Intravenously injected polyplexes and micelles were directly observed by IVRTCLSM. These dynamic states in the bloodstream were compared (Supplementary Videos 1–5). Extracted movie frames at indicated time points are shown in Fig. 1. Immediately after the BPEI/pDNA polyplex was injected, the fluorescence of Cy5 agglomerated into clumps with a variable size in several micrometers range. This nonuniform fluorescence distribution of the polyplex indicated formation of aggregates. PLys/pDNA and PAsp(DET)/pDNA polyplexes showed similar aggregate formation. In contrast, the fluorescence of Cy5 showed uniform distribution when PEG-PLys/pDNA and PEG-PAsp(DET)/pDNA micelles were injected, indicating the absence of aggregates.

3.2. Quantification of aggregates

Using the mean intensity of Cy5 fluorescence, the amount of Cy5-labeled pDNA was evaluated. We acquired the images every 5 s, calculated the relative fluorescence intensity defined as (Cy5 mean fluorescence intensity - Cy5 minimum fluorescence intensity)/(Cy5 maximum fluorescence intensity − Cy5 minimum fluorescence intensity), and plotted the relative fluorescence intensities against time. (Supplementary Fig. 1) The relative fluorescence intensities of naked pDNA decreased immediately, and almost disappeared within 5 min after the start of acquisition. The relative fluorescence intensities of BPEI/pDNA, PLys/pDNA, and PAsp(DET)/pDNA polyplexes also rapidly decreased and dropped to around 0.2 within 10 min after the start of acquisition. In contrast, PEG-PLys/pDNA, and PEG-PAsp(DET)/pDNA polyplex micelles maintained the relative

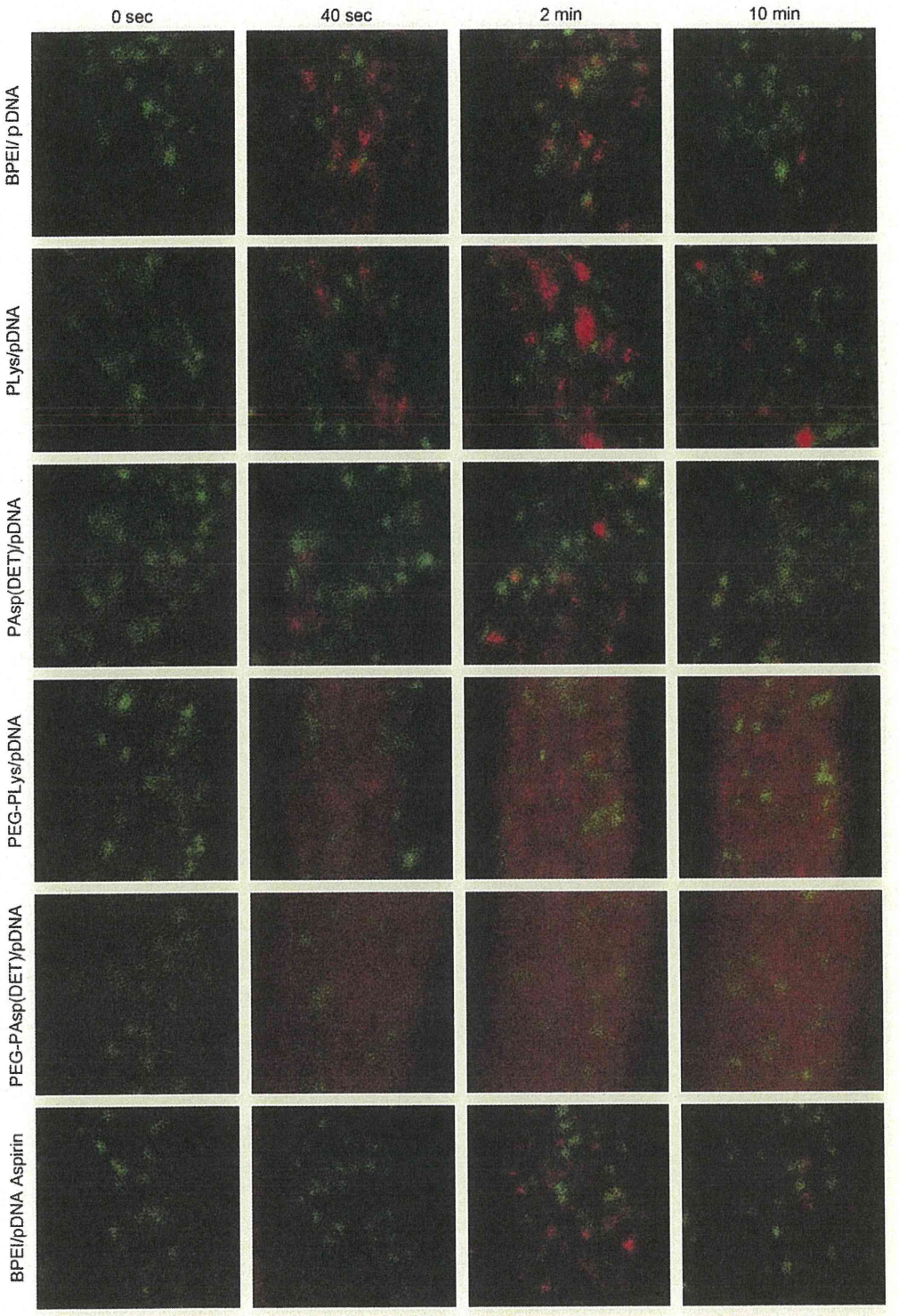

Fig. 1. Intravital confocal micro-videography of polyplexes and polyplex micelles in the bloodstream of the mouse earlobe. Prior to observation, the anti-GPIbβ antibody conjugated with DyLight 488 was injected to label platelets (green). The polyplexes and polyplex micelles incorporating Cy5-labeled pDNA (red) were intravenously injected 10 s after start of observation. Image frames were extracted from videos at identical time points for comparison. Image size: 79.55 μm × 79.55 μm. Confocal slice: 5.11 μm.

fluorescence intensities of around 0.9 and 0.7 even 10 min after the start of acquisition, suggesting the prolonged blood circulation. These results are consistent with the previous studies, which demonstrated pDNA degradation within 5 min and the improvement of blood circulation by PEGylation [17,18].

However, the relative fluorescence intensities could not provide the information about the aggregates of polyplexes and polyplex micelles. Thus, the quantification of aggregates was performed by CV calculation of Cy5 fluorescence in the ROI. The CV is a normalized measure of dispersion of a distribution, and is defined as the ratio of

the standard deviation to the mean. We acquired the images every 5 s, calculated the CV, and plotted the CV against time (Fig. 2). CV values of the polyplexes rapidly increased upon first entry into the vein of the earlobe immediately after intravenous injection. CV values of the polyplexes subsequently fluctuated and decreased over time. In contrast, CV values of the micelles slightly increased upon first entry due to the admixture of micelles and blood, and remained at a plateau at the lower values without fluctuation.

3.3. Platelet interaction study

Platelet is known to be the primary cell components involved in the initial event of thrombosis, and polycations initiate the process of platelet clots formation [19–21]. Thus, in this study, we focused on platelets interaction with cationic polyplexes. To investigate the interaction of polyplexes with platelets, we labeled platelets with DyLight 488-conjugated anti-GPIbβ antibody, and observed the interaction using IVRTCLSM (Fig. 1, Supplementary Videos 1–5). The average labeling efficiency of the antibody has been reported to be ~90% [22]. BPEI/pDNA, PLys/pDNA, and PAsp(DET)/pDNA polyplexes formed aggregates immediately after injection as described above. Their adhesion to platelets was clearly observed approximately 2 min after injection as judged from the colocalization of red and green fluorescences to appear as yellow colored pixels. In contrast, PEG-PLys/pDNA and PEG-PAsp(DET)/pDNA micelles showed no adhesion to platelets throughout the whole experiment.

3.4. Platelet interaction quantification

To quantify the interaction between polyplexes and platelets, we acquired the images every 5 s, and calculated the colocalization between Cy5 fluorescence and DyLight 488 fluorescence using PCC [15]. PCC indicates the intensity of the correlation of two elements, ranging from −1 to +1. The PCC value of the BPEI/pDNA polyplex fluctuated and increased up to approximately 0.4 (Fig. 3). PLys/pDNA and PAsp(DET)/pDNA polyplexes also fluctuated and increased up to approximately 0.25 and 0.33, respectively. In contrast, PCC values of PEG-PLys/pDNA and PEG-PAsp(DET)/pDNA micelles were maintained at almost zero throughout the study.

3.5. Platelet inhibition study

To investigate whether inhibition of platelet function decreases aggregates formation, aspirin was used as an anti-platelet agent. We compared the CV and PCC of the BPEI/pDNA polyplex between aspirin-administered mice and nonadministered control mice (Figs. 1 and 4, Supplementary Video 6). The CV value of the aspirin-administered mice was almost identical to that of control mice; however, their PCC value remained <0.1 throughout the study.

4. Interpretation and significance of new methodologies

Pharmacokinetic studies are indispensable for developing efficient DDSs that transport drugs specifically to the targeted tissue. Pharmacokinetic studies using animals have primarily relied on *ex vivo* techniques, such as analyzing blood or urine samples. These *ex vivo* techniques have been well established to analyze blood circulation, target accumulation, or other pharmacological information of the DDS. However, this approach provides only static information at specific time points. Therefore, investigating dynamic and longitudinal events using this approach is difficult. Alternatively, the intravital microscopy is an emerging technique [23], allowing to investigate such dynamic states of DDS in animals. Recently, we developed the intravital microscopy equipped with fast-scanning laser confocal systems (IVRTCLSM) [9], and demonstrated here its application as a novel tool to dynamically evaluate the interaction between gene vectors and blood components. Our method is characterized by noninvasive observation with high spatial and temporal resolutions to quantitatively monitor the dynamic states

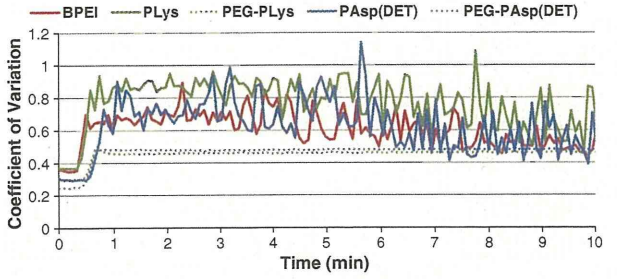

Fig. 2. Quantification of aggregates of polyplexes and micelles. Aggregates of polyplexes and micelles were quantified with CV of Cy5 fluorescence intensities in the frames extracted every 5 s from crude videos.

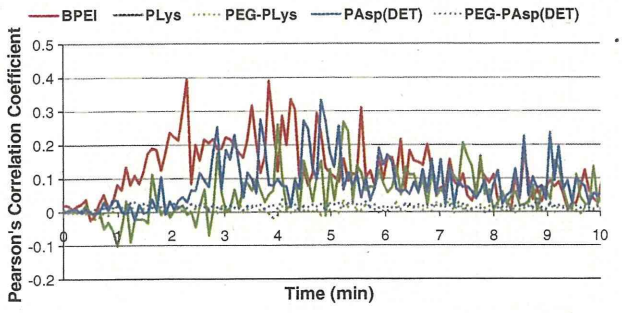

Fig. 3. Quantification of colocalization between polyplexes/micelles and platelets. The colocalization was measured with PCC. PCC was calculated from the frames extracted every 5 s from crude videos.

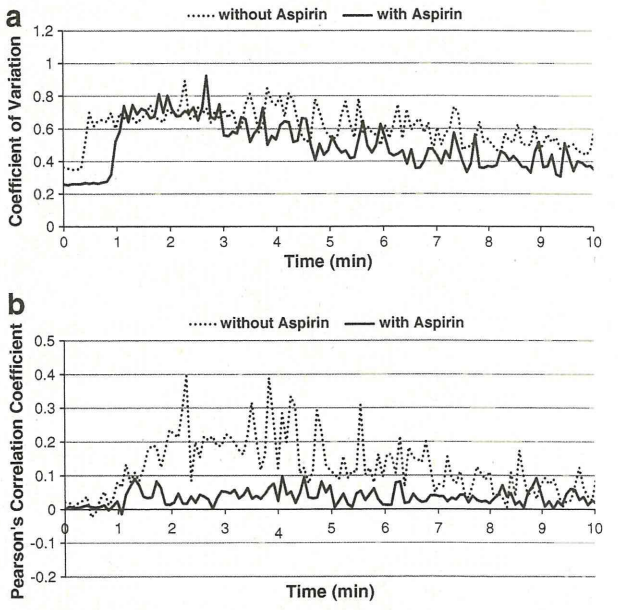

Fig. 4. Platelets inhibition study with aspirin. (a) Aggregates of BPEI/pDNA polyplexes of the aspirin-administered mouse was quantified with the CV of Cy5 fluorescence intensities in the frames extracted every 5 s from crude videos. (b) Colocalization between BPEI/pDNA polyplexes and platelets of the aspirin-administered mouse was quantified with PCC. PCC was calculated from the frames extracted every 5 s from crude videos. For comparison, the CV and PCC of the BPEI/pDNA polyplexes-administered normal mouse in Figs. 2 and 3 were shown respectively again.